

## THE SOURCE REGIONS OF SOLAR ENERGETIC PARTICLES DETECTED BY WIDELY SEPARATED SPACECRAFT

JINHYE PARK<sup>1</sup>, D. E. INNES<sup>2</sup>, R. BUCIK<sup>2</sup>, AND Y.-J. MOON<sup>1</sup>

<sup>1</sup> School of Space Research, Kyung Hee University, Yongin 446-701, Korea; [jinhye@khu.ac.kr](mailto:jinhye@khu.ac.kr)

<sup>2</sup> Max Planck Institute for Solar System Research, D-37191 Katlenburg-Lindau, Germany

Received 2013 April 29; accepted 2013 October 28; published 2013 December 4

### ABSTRACT

We studied the source regions of 12 solar energetic particle (SEP) events seen between 2010 August and 2012 January at *STEREO-A*, *B*, and/or Earth (*Advanced Composition Explorer/Solar and Heliospheric Observatory/GOES*), when the two *STEREO* spacecraft were separated by about 180°. All events were associated with flares (C1 to X6) and fast coronal mass ejections and, except for one, accompanied by type II radio bursts. We have determined the arrival times of the SEPs at the three positions. Extreme ultraviolet (EUV) waves, observed in the 195 Å and 193 Å channels of *STEREO* and the *Solar Dynamics Observatory*, are tracked across the Sun to determine their arrival time at the photospheric source of open field lines connecting to the spacecraft. There is a good correlation between the EUV wave arrival times at the connecting footpoints and the SEP onset times. The delay time between electron onset and the EUV wave reaching the connecting footpoint is independent of distance from the flare site. The proton delay time increases with distance from the flare site. In three of the events, secondary flare sites may have also contributed to the wide longitudinal spread of SEPs.

**Key words:** Sun: activity – Sun: coronal mass ejections (CMEs) – Sun: flares – Sun: magnetic fields – Sun: particle emission

*Online-only material:* color figures

### 1. INTRODUCTION

Solar energetic particle (SEP) flux enhancements occur when particles, accelerated either in a flare or a coronal mass ejection (CME)-driven shock travel along open field lines to their detection point (Cane et al. 1986; Reames 1999; Kallenrode 2003). Most SEPs can be traced to their solar source by considering the spiral structure of the interplanetary magnetic field, the flare site on the Sun, and/or the CME propagation direction. When the onset of SEP events is detected over a large angular range, it has been attributed to acceleration of SEPs at a large CME shock (Dresing et al. 2012; Reames et al. 2012; Rouillard et al. 2012; Tylka et al. 2012; Lario et al. 2013). Now, with the availability of high-cadence, full-Sun extreme ultraviolet (EUV) images from *STEREO* and the *Solar Dynamics Observatory* (*SDO*), we are able to look for connections between widely distributed SEPs and phenomena, such as EUV waves and sympathetic flaring, seen at the solar surface.

To find events with widely distributed SEPs, we use data from the two *STEREO* spacecraft and the *Advanced Composition Explorer* (*ACE*), *Solar and Heliospheric Observatory* (*SOHO*), and *GOES*. The *STEREO* spacecraft have been orbiting the Sun since 2006 December with a separation angle increasing by about 45° per year. By mid 2010, the separation angle was almost 180°. We have looked at SEP events detected in at least two of *STEREO-A* (*STA*), *STEREO-B* (*STB*), and, in the direction of Earth, during the period 2010 August to 2012 January. We have used *ACE*, *GOES*, and *SOHO* to determine SEP fluxes near Earth. Hereafter, we use the term “Earth” to denote any of the spacecraft near Earth (i.e., *ACE*, *GOES*, and *SOHO*). During this period, images with 5 minute cadence from *STEREO* and *SDO* give a complete 360° view of the evolving solar EUV emission so we are able to observe large-scale EUV waves and identify all sources of sympathetic flaring that may produce the wide longitudinal spread of SEPs.

EUV waves are generated in solar eruptions (Thompson & Myers 2009; Warmuth 2010). They show up as faint fronts moving with velocities up to 1000 km s<sup>-1</sup>, with large dimming regions in their wakes. Warmuth & Mann (2011) suggest that the faster ones (> 170 km s<sup>-1</sup>) are real waves and that the slower, more erratic ones are possibly reconnection fronts. It is generally accepted that they track the outer edge of the CME at the Sun (Patsourakos & Vourlidas 2009; Veronig et al. 2010; Rouillard et al. 2012). Whether this edge is a wave front (Thompson et al. 1999; Patsourakos & Vourlidas 2009; Kozarev et al. 2011) or the rim of the region affected by magnetic reconfiguration associated with a CME (Attrill et al. 2007; Cheng et al. 2012) is often not resolvable.

Even though the cause of EUV waves is not fully understood, previous studies have shown a connection between EUV wave propagation and the generation of SEPs. It was reported that the propagation of Moreton waves, which were likely accompanied by EUV waves, was associated with the generation of SEPs (Kocharov et al. 1994; Torsti et al. 1998, 1999). Krucker et al. (1999) showed that EUV waves are the most likely source of impulsive electron events, when the arrival of electrons is significantly delayed with respect to the onset of the associated type III radio burst. Vainio & Khan (2004) considered coronal shocks that can be excited by slow CMEs and flares, not just fast CMEs. These shocks may be refracted back toward the solar surface so that the interplanetary medium is connected to the plasma downstream of the shock. Thus, diffusive shock acceleration could explain the observed power-law ion spectra. A detailed observational study by Rouillard et al. (2012) of the event on 2011 March 21, which is also included in our study, showed that for a fast CME, the EUV wave tracks the extent of the high-pressure variations developing around the expanding CME and that the wave is associated with a shock capable of accelerating particles. Here, we consider the EUV wave as an indicator of the angular spread of the CME and look at when the EUV wave reaches the magnetic connection

points of the *STEREO* and Earth spacecraft at the solar surface.

The interplanetary magnetic field emanates from the footpoints of coronal holes and streamers. Potential field source surface (PFSS) models give a good approximation of the magnetic field up to  $2.5 R_{\odot}$  and can be used to trace back the sources of the interplanetary field from this distance (Neugebauer et al. 1998). Further out, the field is stretched by the solar wind to form the Parker spiral and so depends on the solar wind speed.

Since released SEPs follow the magnetic field as long as interplanetary scattering is not a dominant effect, it is reasonable to assume that there may be a relationship between the time that the EUV wave crosses the spacecraft connection point at the Sun and the arrival time of SEPs at the connected spacecraft. If the EUV wave front is triggering reconnections, then SEPs may be released from the reconnection site. Alternatively, if the EUV wave is the skirt of the shock, it should give a good indication of the time the edge of the shock reached the connecting field line. The main motivation for this study is to see if such a relationship exists by considering as many events with widely separated SEPs as we could find during the time when the *STEREO* spacecraft were about  $180^{\circ}$  apart.

Furthermore, SEP events are affected by pre-event solar activity. Gopalswamy et al. (2004) and Kahler (2005) found that CMEs following within a day of another wide CME are more likely to be associated with high-intensity SEP events. This is probably because there are more seed particles and efficient particle acceleration downstream of the first CME (Li et al. 2012a; Nitta et al. 2012).

This paper is structured as follows. In Section 2, we describe the data. Source regions related to the SEP events are elaborated in Section 3. In Section 4, we discuss SEP flux enhancements and the influence of magnetic field connection, EUV wave direction, and pre-event solar activity. We summarize our results in Section 5.

## 2. OBSERVATIONS

We have selected 12 events that show almost simultaneous SEP flux enhancements in at least two of *STA*, *STB*, and Earth (*ACE*, *GOES*, and *SOHO*) when the *STEREO* spacecraft were about  $90^{\circ}$  from the Earth–Sun line. We obtained electron fluxes from the Solar Electron Proton Telescope (SEPT; Müller-Mellin et al. 2008) on *STEREO* averaged over 5 minutes in four low-energy channels (55–65 keV, 105–125 keV, 195–225 keV, and 335–375 keV) and from the High Energy Telescope (HET; von Rosenvinge et al. 2008) in three energy channels (0.7–1.4 MeV, 1.4–2.8 MeV, and 2.8–4.0 MeV). We also used the *ACE* Electron, Proton, and Alpha Monitor (EPAM; Gold et al. 1998) averaged over 5 minutes in four energy channels (38–53 keV, 53–103 keV, 103–175 keV, and 175–315 keV) and the *SOHO* Electron Proton and Helium Instrument (EPHIN; Müller-Mellin et al. 1995) in two channels (0.67–3.0 MeV and 2.64–10.4 MeV). Proton fluxes are from the Low Energy Telescope (LET; Mewaldt et al. 2008) on *STEREO* averaged over 10 minutes in three energy channels (1.8–3.6 MeV, 4–6 MeV, and 6–10 MeV), from HET in four high-energy channels (13.6–15.1 MeV, 20.8–23.8 MeV, 29.5–33.4 MeV, and 40.0–60.0 MeV), the Energetic and Relativistic Nuclei and Electron instrument (ERNE; Torsti et al. 1995) on *SOHO* averaged over 10 minutes in seven channels (1.90–3.06 MeV, 3.06–5.12 MeV, 5.12–8.69 MeV, 8.69–14.9 MeV, 12.6–20.8 MeV, 19.4–32.2 MeV, and 32.2–57.5 MeV).

The solar sites were identified in full-Sun EUV Stonyhurst Heliographic (Earth-view) images. For each event, we combined the two *STEREO* Extreme Ultraviolet Imager (EUVI; Wuelser et al. 2004) 195 Å images with the nearest in time *SDO*/Atmospheric Imaging Assembly (AIA) 193 Å image to make movies of the events with a cadence of 5 minutes over a period of 6 hr, starting about 1 hr before the event time. The EUV waves are usually faint in the intensity images, so we constructed running ratio movies as the log of the intensity ratios of consecutive images. These are optimal for viewing the EUV waves and small flares because they show relative changes and bright, quiescent active regions (ARs) disappear. The connection points of the spacecraft have been obtained using synoptic magnetic field and ecliptic-plane PFSS extrapolations from the GONG Web site (<http://gong.nso.edu/data/magmap/pfss.html>). The images provided by the site have been rotated to Stonyhurst coordinates. The original connection points for Earth, *STA*, and *STB* longitudes shown on the plots do not account for the Parker spiral. Therefore, we have moved the connection points at  $2.5 R_{\odot}$ , westward according to the solar wind speed observed at the time of the events using the equation

$$\phi_0 = D\Omega/V_w + \phi, \quad (1)$$

where  $\phi$  and  $\phi_0$  are the spacecraft and solar longitudes,  $D$  is the distance to the Sun,  $V_w$  is the solar wind speed obtained from *ACE* Solar Wind Electron Proton Alpha Monitor (McComas et al. 1998) and *STEREO* Plasma and Suprathermal Ion Composition (Galvin et al. 2008) measurements, and  $\Omega$  is the solar rotation rate based on a Carrington period of 27.3 days.

Additional information on the events has been extracted from the *GOES* flare list (<http://solar-center.stanford.edu/SID/activities/PickFlare.html>), the *SOHO* LASCO CME catalog ([http://cdaw.gsfc.nasa.gov/CME\\_list](http://cdaw.gsfc.nasa.gov/CME_list)), the CACTus COR2 CME list (<http://sidc.oma.be/cactus>), the type II radio burst lists compiled by the *Wind* and *STEREO* data center ([http://ssed.gsfc.nasa.gov/waves/data\\_products.html](http://ssed.gsfc.nasa.gov/waves/data_products.html)), and type III radio burst data (<http://secchirh.obspm.fr>).

## 3. DESCRIPTION OF THE EVENTS

For each event, we present: (1) the proton and electron flux measured at each spacecraft with the times of CMEs indicated, (2) a PFSS field extrapolation and magnetic field plot with the source regions and spacecraft connection points marked, (3) a ratio image of the Sun at the time of the EUV wave showing the positions of space–time cuts in the direction of the footpoints of the connecting open field line to each spacecraft, and (4) the space–time running ratio images along those cuts.

In the PFSS images, green represents positive polarity and red negative polarity fields. The open magnetic field lines reaching to the ecliptic-plane flux are represented as lines and other coronal hole fields are represented as dots. The polarity inversion line (blue) divides the surface into same-polarity groups. On the space–time images, we have marked the wave speed and the positions of the connecting footpoint for the different spacecraft. Here, “E” stands for Earth and “A” is for *STA* and “B” is for *STB*. Six of the events are described in more detail in the main text and the others are described in the Appendix.

We have summarized the properties of the 12 SEP events in three tables. Table 1 lists the 12 SEP events and their associated solar phenomena. The events are related to flares ranging from C1 to X6 in X-ray strength and fast CMEs ranging from 1005 km s<sup>−1</sup> to 2256 km s<sup>−1</sup> with an average speed of

**Table 1**  
The Solar Sources of the 12 SEP Events

Event	Date	Flare <sup>a</sup> Start	Max	Class	Location	AR	CME <sup>b</sup> Time	$V$ (km s <sup>-1</sup> )	Radio <sup>c</sup> II Time	Radio <sup>d</sup> III Time	EUV <sup>e</sup> $V$ (km s <sup>-1</sup> )
1	20100814	09:38	10:05	C4.4	N17W52	11099	10:12 <sup>L</sup>	1205 <sup>L</sup>	10:00	09:55	310
2	20100818	04:45	05:48	C4.5	N17W91	11099	05:24 <sup>A</sup>	1250 <sup>A</sup>	06:05	05:30	200
3	20110307	19:43	20:12	M3.7	N24W59	11164	20:00 <sup>L</sup>	2256 <sup>L</sup>	20:00	19:50	510
4	20110321	02:04	...	...	N22W132	...	02:24 <sup>B</sup>	1562 <sup>B</sup>	02:20	02:20	528
5	20110804	03:41	03:57	M9.3	N15W49	11261	03:54 <sup>A</sup>	1785 <sup>A</sup>	04:15	03:50	510
6	20110809	07:48	08:05	X6.9	N17W83	11263	08:12 <sup>L</sup>	1610 <sup>L</sup>	08:20	08:00	420
7	20110921	21:35 <sup>f</sup>	...	...	N15W120	...	22:12 <sup>L</sup>	1007 <sup>L</sup>	...	21:40?	225
8	20110922	10:28	11:01	X1.4	N11E74	11302	10:48 <sup>L</sup>	1905 <sup>L</sup>	11:05	10:40	760
9	<u>20111103</u>	21:40	...	...	N05E160	...	22:54 <sup>A</sup>	1136 <sup>A</sup>	22:35	22:15	473
		22:28	22:35	C5.8	N18E60	11339	...	...	...	...	...
		22:12	22:18	C5.4	N10W85	11333	...	...	...	...	...
10	<u>20111126</u>	06:40	07:10	C1.2	N08W49	11353	07:12 <sup>B</sup>	1005 <sup>B</sup>	07:15	07:10	380
11	20120123	03:38	03:59	M8.7	N28W36	11402	03:54 <sup>B</sup>	1785 <sup>B</sup>	04:00	03:40	525
12	20120127	17:37	18:37	X1.7	N27W71	11402	18:27 <sup>L</sup>	1136 <sup>L</sup>	18:30	18:15	715

**Notes.** The underlined events are likely related to multiple source regions.

<sup>a</sup> Flare times are taken from [ftp://ftp.ngdc.noaa.gov/STP/space-weather/solar-data/solar-features/solar-flares/x-rays/goes](http://ftp.ngdc.noaa.gov/STP/space-weather/solar-data/solar-features/solar-flares/x-rays/goes).

<sup>b</sup> CME time is the appearance in LASCO C2 or SECCHI COR2 field of view. CME times are taken from [http://cdaw.gsfc.nasa.gov/CME\\_list](http://cdaw.gsfc.nasa.gov/CME_list) and <http://secchi.nrl.navy.mil/cactus>. L is SOHO/LASCO. A and B are STA/COR2 and STB/COR2, respectively.

<sup>c</sup> Radio II times are taken from [http://ssed.gsfc.nasa.gov/waves/data\\_products.html](http://ssed.gsfc.nasa.gov/waves/data_products.html) except for 20100814, which was taken from <http://secchirh.obspm.fr>.

<sup>d</sup> Radio III times are taken from <http://secchirh.obspm.fr>.

<sup>e</sup> EUV wave speeds are the average speeds from the source to the spacecraft connecting points.

<sup>f</sup> The brightening was observed around the west limb at 21:35 UT on 2011 September 21.

**Table 2**  
The Spacecraft Ecliptic Plane Connection Points, the SEP Onset Times, and the EUV Wave Arrival Times

Date	STB	Earth	STA	STB	Electron Earth (335–375 keV)	STA (175–315 keV)	STB (335–375 keV)	Proton Earth (1.8–3.6 MeV)	STA (1.90–3.06 MeV)	STB (1.8–3.6 MeV)	EUV Earth	STA
20100814	9W	57W	142W	10:44	10:37	**10:50	*12:47	*10:45	*13:28	*10:00	09:30	**10:00
20100818	9W	57W	137W	06:42	05:57	05:57	09:55	*07:24	08:28	*06:20	05:00	05:00
20110307	34E	56W	142W	20:06	*20:24	20:58	... <sup>a</sup>	**20:48	22:10	*20:30	19:50	20:00
20110321	37E	56W	142W	...	02:52	02:26	...	*03:30	03:17	...	*02:40	*02:20
20110804	32E	57W	155W	*06:12	04:06	*06:17	*07:23	06:27	*08:24	04:30	03:55	*04:30
20110809	46E	38W	149W	CIR	08:05	08:45	CIR	09:16	...	**08:20	08:00	*08:30
20110921	35E	57W	158W	22 04:23	*21 23:13	21 23:05	...	**22 02:54	22 00:54	...	**22:20	21:30
20110922	35E	57W	158W	10:45	*12:12	12:36	11:17	**13:38	**14:20	10:30	**11:15	...
<u>20111103</u>	37E	56W	178W	3 23:14	3 22:39	3 22:25	*4 02:08	**4 02:24	*4 00:45	...	...	22:10
<u>20111126</u>	40E	56W	158W	07:44	07:12	08:52	09:58	08:24	14:24	...	06:55	...
20120123	49E	74W	151W	05:15	03:50	*05:29	08:59	06:03	06:20	04:10	03:55	...
20120127	65E	56W	162W	...	18:28	20:20	...	19:40	...	18:50	18:10	18:40

**Notes.** The travel time of a 175 keV electron is  $\Delta t = 15$  minutes. The travel time of a 1.8 MeV proton is  $\Delta t = 161$  minutes. The travel time of a photon is  $\Delta t = 8.3$  minutes. The number of asterisks by the SEP times indicates the temporal binning used to obtain the time. The asterisks by the EUV wave times indicate the accuracy of the EUV wave arrival time (5, 10, or 20 minutes). CIR means particles in a corotating interaction region.

<sup>a</sup> It has ~60 minutes uncertainty due to the previous event.

1470 km s<sup>-1</sup>. All are accompanied by a type III radio burst and all but one are accompanied by a type II radio burst. The underlined event appears to have been caused by flares in more than one AR, although there was only one EUV wave, CME, and type II burst. The average EUV wave speeds, computed from the space–time images, are given in Table 1. More accurate wave speeds along different directions are given in the space–time images related to individual events.

Table 2 lists the connecting longitudes at 2.5  $R_{\odot}$  for the three spacecraft. These were calculated using the simple Parker spiral field formula (Equation (1)). Table 2 also lists the SEP onset times at the spacecraft and the EUV wave arrival times at their connecting footpoints. Some event onsets were easier to see in the low-energy channels and others in the high-energy ones.

ACE electron onset is given in the 175–315 keV channel and SOHO proton onset is given in the 1.90–3.06 MeV channel. STEREO onsets are obtained from the 335–375 keV channel for electrons and from the 1.8–3.6 MeV channel for protons. If the onset is not seen in these channels due to strong background, we obtained the onset time from a higher energy channel. We then estimated the onset time for the reference low-energy channel, assuming a travel distance of 1.2 AU, so that we can compare delay times of all events. The onset time is not always easy to determine. At first, we looked at the flux profiles from low to high energy bands to get a crude estimate of the onset time. Then, we plotted the data around the time at which the flux increase occurred. We found the three earliest consecutive times with increasing flux and marked the first of

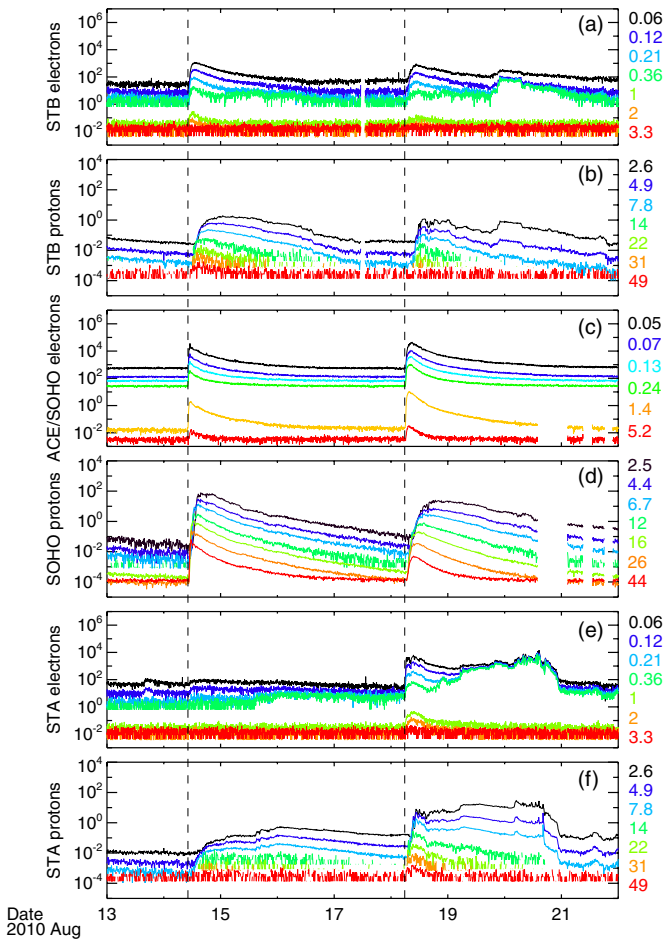


**Figure 1.** 2010 August 14 and 18 SEP events. The fluxes are in units of particles  $\text{cm}^{-2} \text{s}^{-1} \text{sr}^{-1} \text{MeV}^{-1}$ . (a) Electron fluxes in seven energy channels measured by *STB* SEPT and HET, (b) proton fluxes in seven energy channels measured by *STB* LET and HET, (c) electron fluxes in six energy channels measured by *ACE* EPAM and *SOHO* EPHIN, (d) proton fluxes in seven energy channels measured by *SOHO* ERNE, (e) electron fluxes in seven energy channels measured by *STA* SEPT and HET, and (f) proton fluxes in seven energy channels measured by *STA* LET and HET. The numbers shown on the right axis are the middle of the energy ranges in MeV. The first dashed line is the CME at 10:12 UT on August 14 and second dashed line is the CME at 05:24 UT on August 18.

(A color version of this figure is available in the online journal.)

these three as our onset time. If the data were very noisy and there were no three consecutive times with increasing flux, we doubled the time over which the data were averaged until an enhancement time emerged. If the data was very noisy and there were no three consecutive times with increasing flux, we doubled the time over which the data was averaged until an enhancement time emerged. The number of binnings is indicated by the number of asterisks by the times in Table 2.

The arrival times of the EUV waves are the times that the leading edges of the EUV waves reached the footpoints of the open field lines extending to the connecting longitudes of the spacecraft, given in Columns 11–13 of Table 2. There are several significant sources of uncertainty with these times. They depend strongly on the applicability and accuracy of the PFSS extrapolations and the Parker spiral formula for pinpointing the footpoints of the connecting field lines. A feel for the reliability of the positions can best be obtained by looking at the PFSS extrapolations and the spacecraft connecting points for the individual events. In many cases, the spacecraft connecting

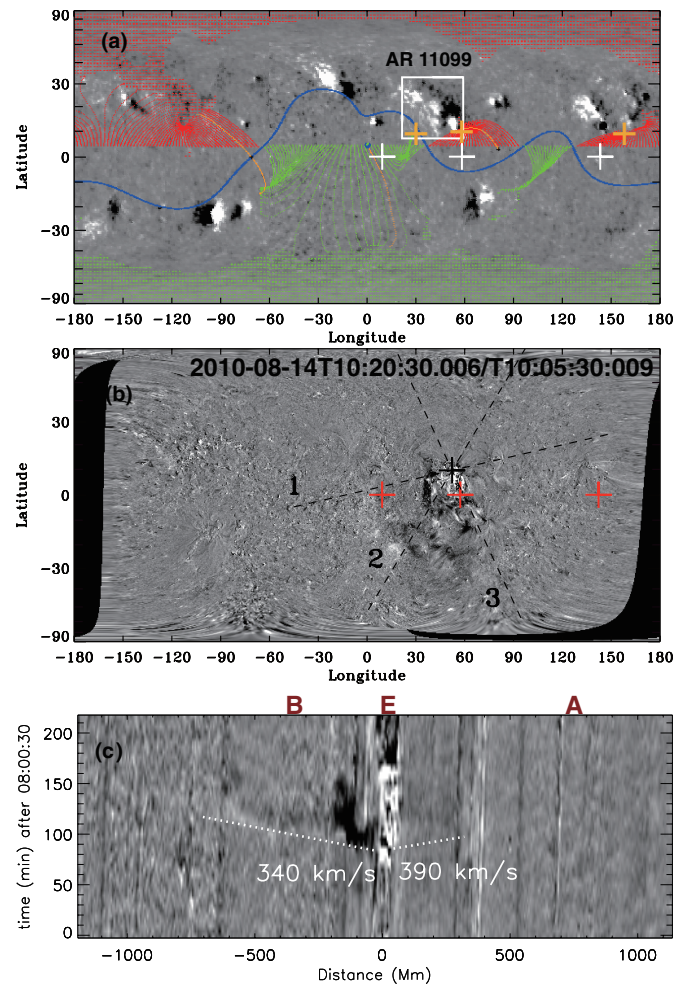


**Figure 2.** 2010 August 14 source region and EUV wave: (a) GONG synoptic magnetic field with PFSS ecliptic plane field lines traced back to their source. White and red crosses mark the longitudes of *STB*, Earth, and *STA* at  $2.5 R_{\odot}$ . The photospheric footpoints of the connecting field lines are marked by orange crosses. Connecting footpoints are deduced by tracing the field lines from the white crosses to the Sun. Green/red indicates positive/negative open fields. The source region is enclosed by a white square. (b) Full Sun ratio image at the times given. This is a composite of *STB* 195 Å, *SDO* 193 Å, and *STA* 194 Å images. The dashed line indicates the position of the space-time image below. (c) Running ratio space-time image along the line in (b). The white number is the approximate wave speed calculated by manually choosing the start and end positions of the wave.

(A color version of this figure is available in the online journal.)

point lies close to the separatrix between two possible footpoint regions. In these cases, we chose the footpoints closest to EUV wave onset site. The EUV wave arrival time is determined by looking at the running ratio movies and seeing when the wave arrives at the footpoint site and, for confirmation, by linear extrapolation of the EUV wavefront in the running ratio space-time images to the footpoint site. Times to sites close to the EUV wave source are accurate to within 5 minutes, but the further the connecting footpoint is from the source, the more difficult it is to determine the wave arrival time. The times to the more distant sources are accurate to within 20 minutes. The accuracy of the EUV arrival times is indicated by asterisks in Table 2.

Table 3 represents the source region connections with the spacecraft. A “✓” indicates direct connection to the spacecraft. The magnetic polarity (positive/negative) of the connecting region is given in brackets.

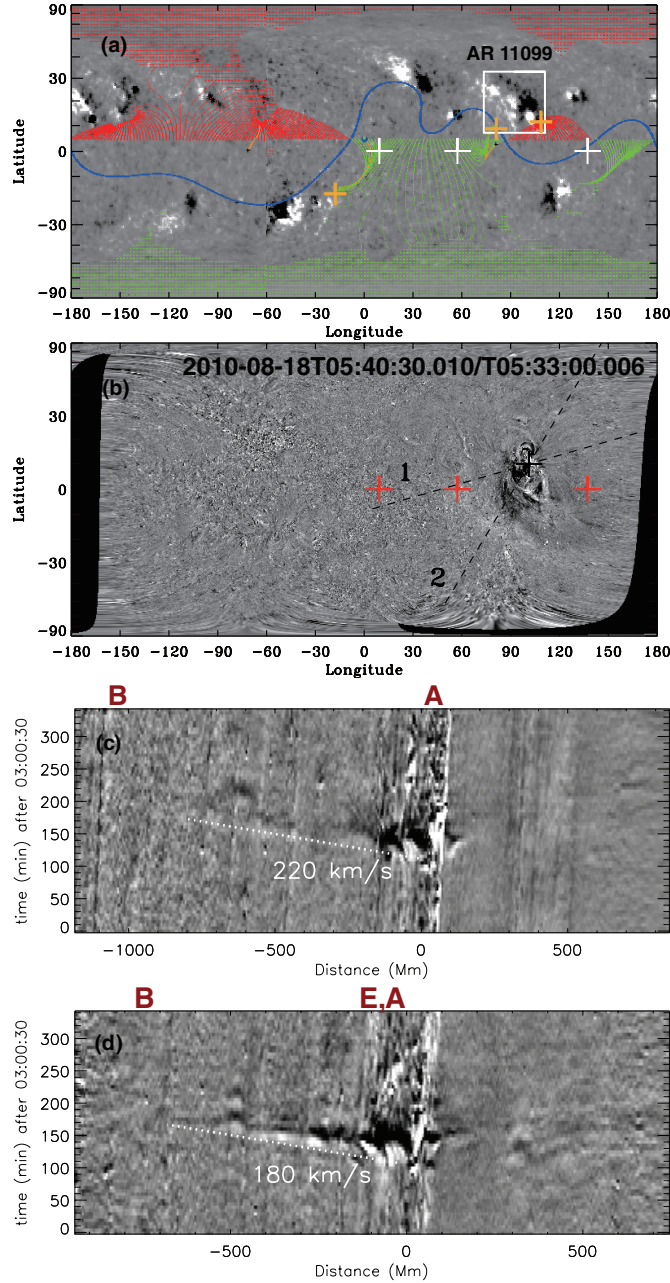


**Figure 3.** 2010 August 18 source region and EUV wave: (a) synoptic ecliptic-plane PFSS image as described in Figure 2, (b) ratio image, as in Figure 1, (c) running ratio space-time image along line 1, and (d) running ratio space-time image along line 2.

(A color version of this figure is available in the online journal.)

### 3.1. The Events from Single Source Regions

Most events are from a single source. We describe two examples that occurred from the same AR (AR 11099) with an interval of about 4 days between them. There were no intervening fast CMEs and it is unlikely that the first had a direct influence on the SEP acceleration rate of particles in the second. Figure 1 shows electron and proton fluxes from 2010 August 13 to 21 at *STB*, *ACE/GOES/SOHO*, and *STA*. The fluxes were enhanced in all spacecraft on both days.

#### 3.1.1. The Event of 2010 August 14

This event was associated with a C4.4 flare in an AR near N17W52, a westward, from Earth, CME with velocity

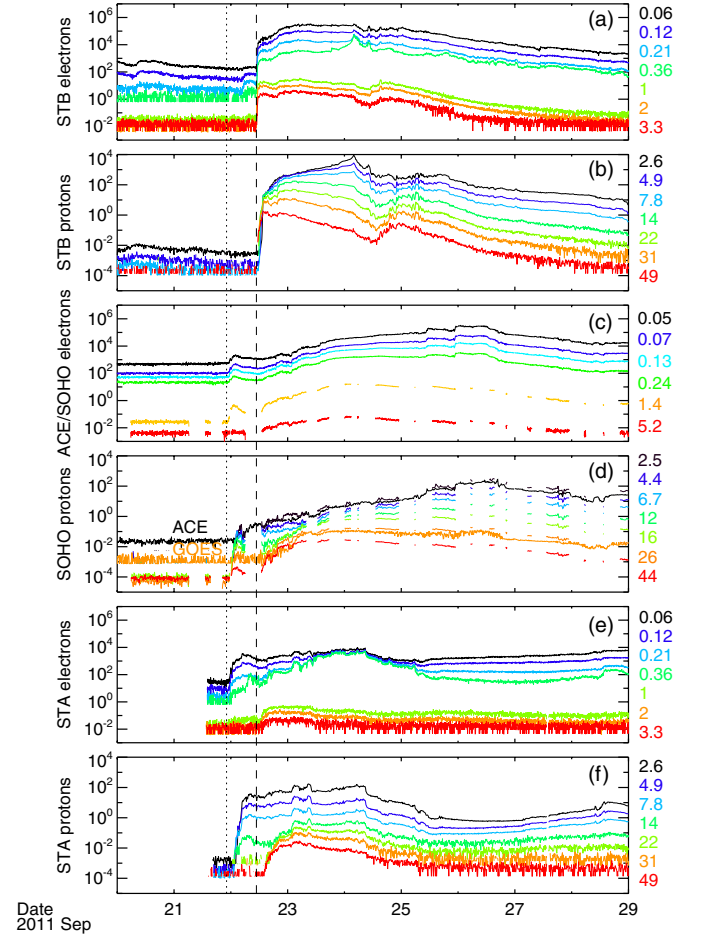


**Figure 4.** 2011 September 21 and 22 SEP events, as in Figure 1. In addition, in (d) we show the *ACE* 1.89–4.74 MeV and *GOES* > 30 MeV fluxes. The dotted line represents the CME at 22:12 UT on September 21 and the dashed line represents the CME at 10:48 UT on September 22.

(A color version of this figure is available in the online journal.)

**Table 3**  
Source Region Connections with the Spacecraft

Date	<i>STB</i>	Earth	<i>STA</i>
20100814	✓ (P)	✓ (N)	— (N)
20100818	... (P)	✓ (P)	✓ ? (P,N)
20110307	... (P)	✓ (N)	... ? (N)
20110321	... (P)	... (N)	✓ ? (P)
20110804	... (P)	✓ (P,N)	... (N)
20110809	CIR (N)	✓ (P)	... (N)
20110921	... (P)	... (N)	✓ (N)
20110922	✓ (P)	... (N)	... (N)
20111103	✓ (N)	✓ (P)	✓ (N)
20111126	... (P)	✓ (N)	... (P)
20120123	... (P)	... (P)	... (N)
20120127	... (N)	✓ (P)	... (N)

**Notes.** “P” in brackets signifies positive polarity and “N” signifies negative polarity. The question marks indicate unclear cases. CIR means particles in a corotating interaction region.

1205 km s<sup>-1</sup> and a type II radio burst. The PFSS extrapolation in Figure 2(a) shows that Earth was directly connected via a negative (red) magnetic field to the source region. The *STB* was connected via a positive magnetic field to a region a few degrees to the southeast and the *STA* connection site is about 100° west of the flare. The direction and speed of the EUV wave can be seen

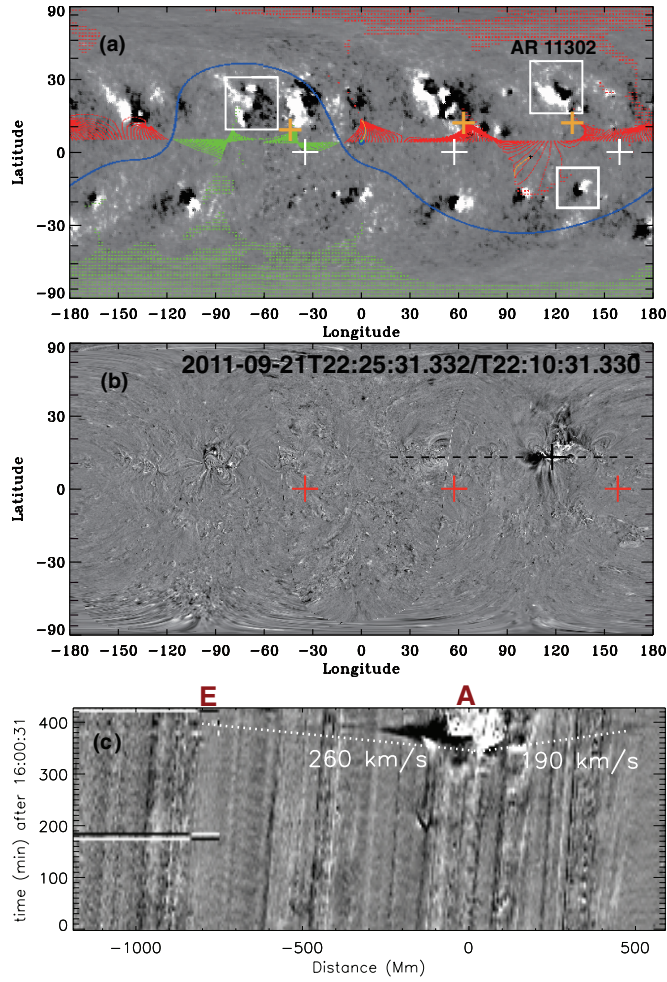


**Figure 5.** 2011 September 21 and 22 source regions and 2011 September 21 EUV wave: (a) GONG magnetic field map as described in Figure 2. The September 21 source was around N15W120. The main source on September 22 was around N11E74. There was a second source around S15W135. (b) Ratio image and EUV wave on September 21. (c) Running ratio space-time image along the dashed line in (b).

(A color version of this figure is available in the online journal.)

in the running ratio images (Figures 2(b) and (c)). We calculated the EUV wave velocity along a line connecting the footpoints of *STB* and *STA* and passing through the source region. The wave passed the connection points of Earth and *STB* at 09:40 UT and 10:00 UT, respectively. The highest velocity is  $390 \text{ km s}^{-1}$  in the direction of the negative field connecting to *STA*. The wave in this direction is very faint and seems to disappear before reaching the connecting footpoint. We therefore consider the possibility that *STA* was connected via the positive field to the AR to the south of the flare site. The EUV wave reaches this site at 10:00 UT.

### 3.1.2. The Event of 2010 August 18

The event source was a C4.5 flare and fast CME ( $1250 \text{ km s}^{-1}$ ) from an AR around the west limb, as seen from Earth. A type II radio burst was observed at the same time as the CME. Figure 3(a) shows that the magnetic fields of the source region were directly connected to *STA* via negative flux. Earth was connected via positive flux to a site a short distance (50 Mm) southeast of the flare. As on the August 14 event, the EUV wave mainly propagated from the source region southward. There are two possible footpoint regions for the *STB* connection: the

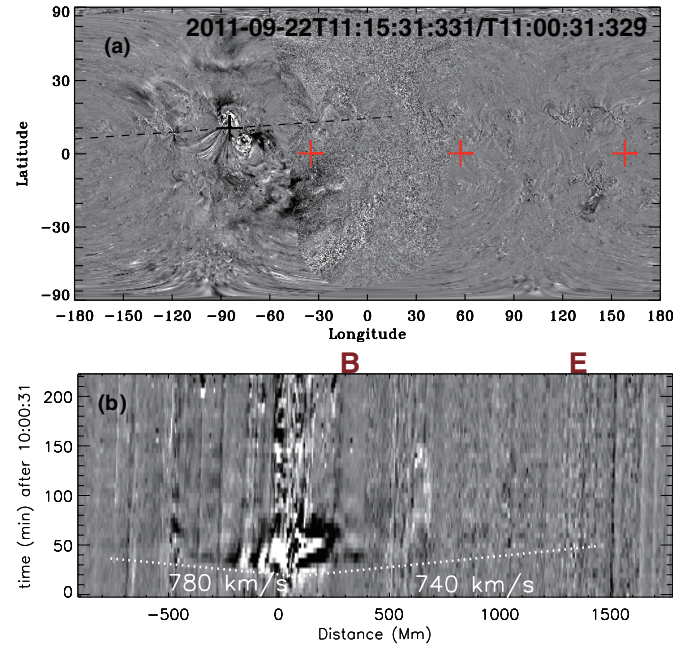


**Figure 6.** 2011 September 22 EUV wave: (a) ratio images for September 22. (b) Running ratio space-time image along the dashed line in (a).

(A color version of this figure is available in the online journal.)

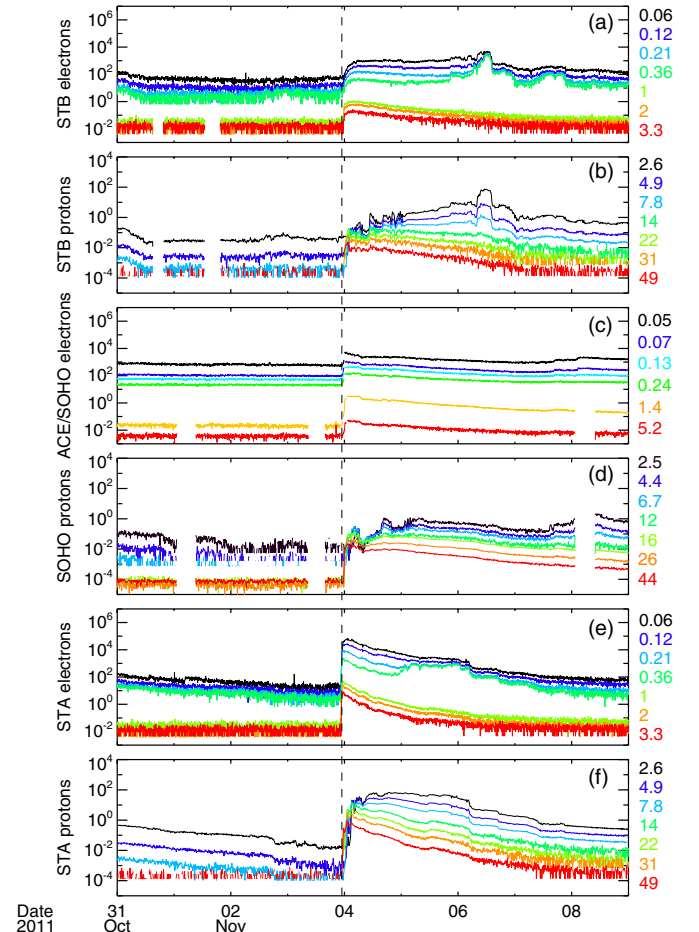


**Figure 7.** 2011 November 3 SEP event, as in Figure 1. The dashed line represents the CME at 22:54 UT on November 3.

(A color version of this figure is available in the online journal.)

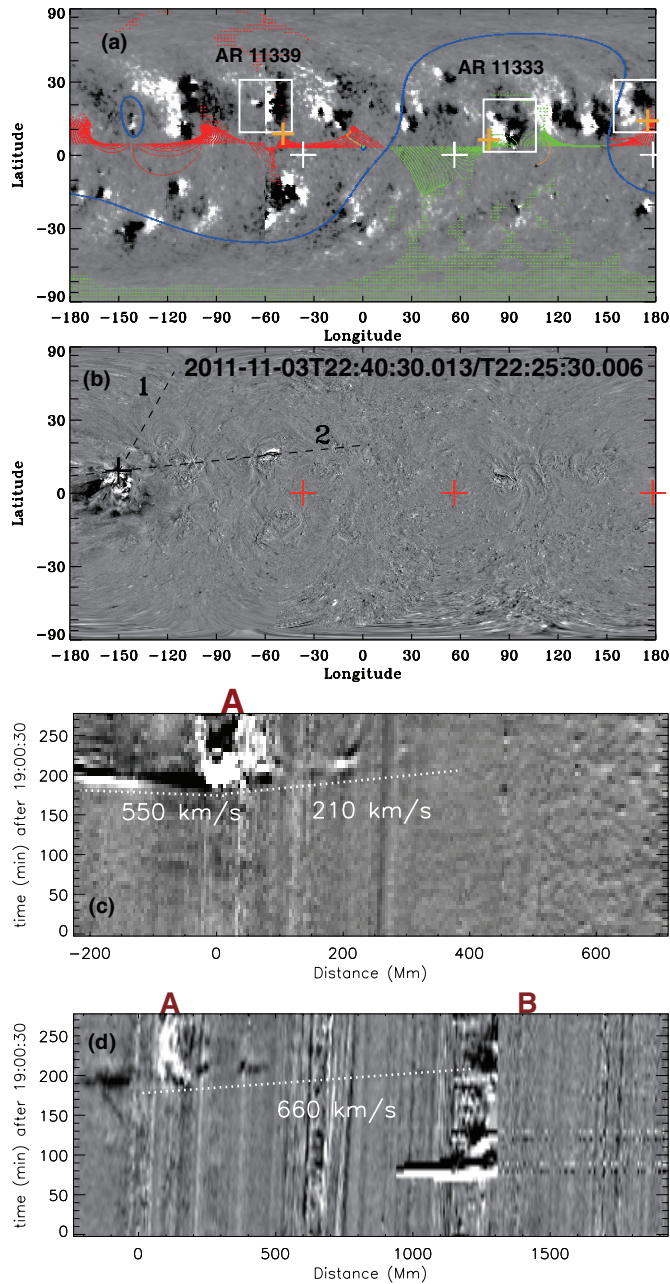


**Figure 8.** 2011 November 3 source regions and EUV wave. (a) Synoptic ecliptic-plane PFSS image as in Figure 2. The source region at N10W180 should be at N10E160 but the GONG synoptic map is not accurate for backside ARs. (b) Ratio image, as described in Figure 1. (c) Running ratio space-time image along line 1. (d) Running ratio space-time image along line 2.

(A color version of this figure is available in the online journal.)

southern coronal hole and the AR around S30E60. The EUV wave reached both points at around the same time, 6:20 UT.

### 3.2. Events with Multiple Source Regions

#### 3.2.1. Events of 2011 September 21 and 22

This was a double CME/SEP event (Figures 4–6). The first was a fast CME ( $1007 \text{ km s}^{-1}$ ) associated with a brightening seen by *STA* on 2011 September 21 at 21:35 UT around W120°. This produced SEP flux enhancements at *STA* and, slightly delayed and weaker, at Earth. SEPs were not detected in the high-energy channels. The second CME with almost twice the speed ( $1905 \text{ km s}^{-1}$ ) and was associated with an X1 flare on

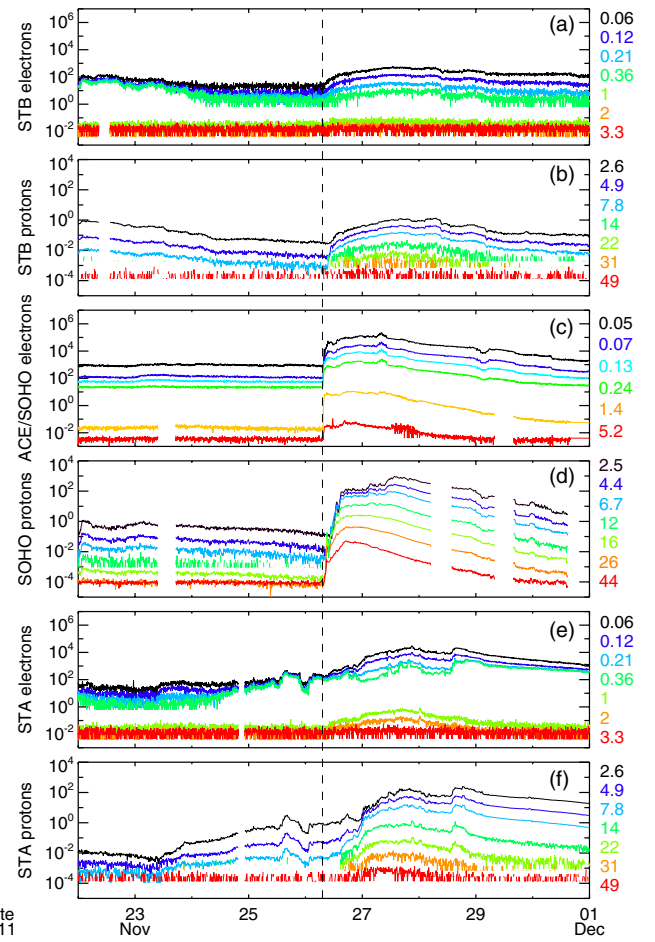


**Figure 9.** 2011 November 26 SEP event as in Figure 1. The *STA* SEPT (low-energy) electron fluxes were affected by ion contamination in the instrument (see <http://www2.physik.uni-kiel.de/stereo/browseplots/>) throughout most of November 26. The dashed line represents the CME at 07:12 UT on November 26.

(A color version of this figure is available in the online journal.)

2011 September 22 at 10:28 UT from N11E74. This produced clear SEP enhancements at *STB* at both high and low energies. At Earth and *STA*, only the high-energy onsets were well defined, probably due to the relatively high background in the low-energy channels from the first event on September 21.

As shown in Figure 5(a), the source of the first SEP event was directly connected to *STA* and this explains the rapid flux enhancement at *STA*. The EUV wave associated with this event was relatively slow ( $225 \text{ km s}^{-1}$ ) and reached the Earth footprint 1 hr after the initial brightening (Figure 5(c)), which is consistent with the SEP delay at Earth.

The second CME was associated with a fast ( $760 \text{ km s}^{-1}$ ) EUV wave launched from the site of the powerful X1 flare. The source of the second event does not seem to be directly connected to *STB* (Figure 5(a)), but the EUV wave reaches the *STB* footprint 10 minutes after the flare, so this can explain the immediate flux enhancements measured at *STB*. The wave reached the Earth footprint 45 minutes after the flare (Figure 6(b)) and faded before reaching the connecting footprint of *STA*. There was a third EUV wave associated with a brightening at 11:45 UT from the small AR at S15W135 in Figure 5(a). An EUV wave travelling at  $760 \text{ km s}^{-1}$  would have reached this site from the X-flare site (N11E74) in about

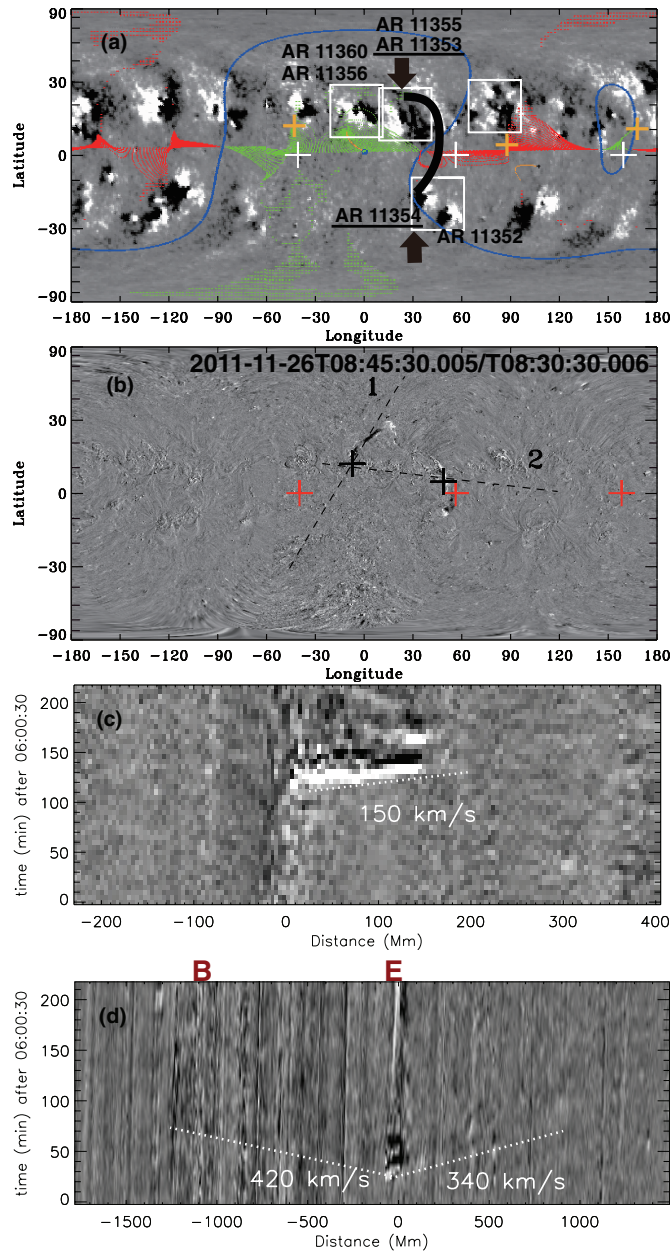


**Figure 10.** 2011 November 26 source sites and EUV waves. (a) GONG magnetic field map, as described in Figure 2. The thick black line represents a filament that erupted. The flaring ARs are labeled. (b) Ratio of images at the given times, as in Figure 2. The two black crosses mark the onset site of the jet shown in (c) and the EUV wave shown in (d). (c) Running ratio space-time image along line 1 in (b). (d) Running ratio space-time image along line 2 in (b). (A color version of this figure is available in the online journal.)

40 minutes so there may have been a connection between the X-flare and this small AR.

This was a complicated series of events. Although the two main eruptions were almost  $180^\circ$  and 13 hr apart, it is possible that SEPs accelerated in the second event propagated through regions of the heliosphere affected by the first event and that this caused the high-energy flux enhancements at *STA* and Earth associated with the second event.

### 3.2.2. The Event of 2011 November 3

In this event, SEP fluxes suddenly increased in all spacecraft without a longitudinal dependence, except for the proton fluxes

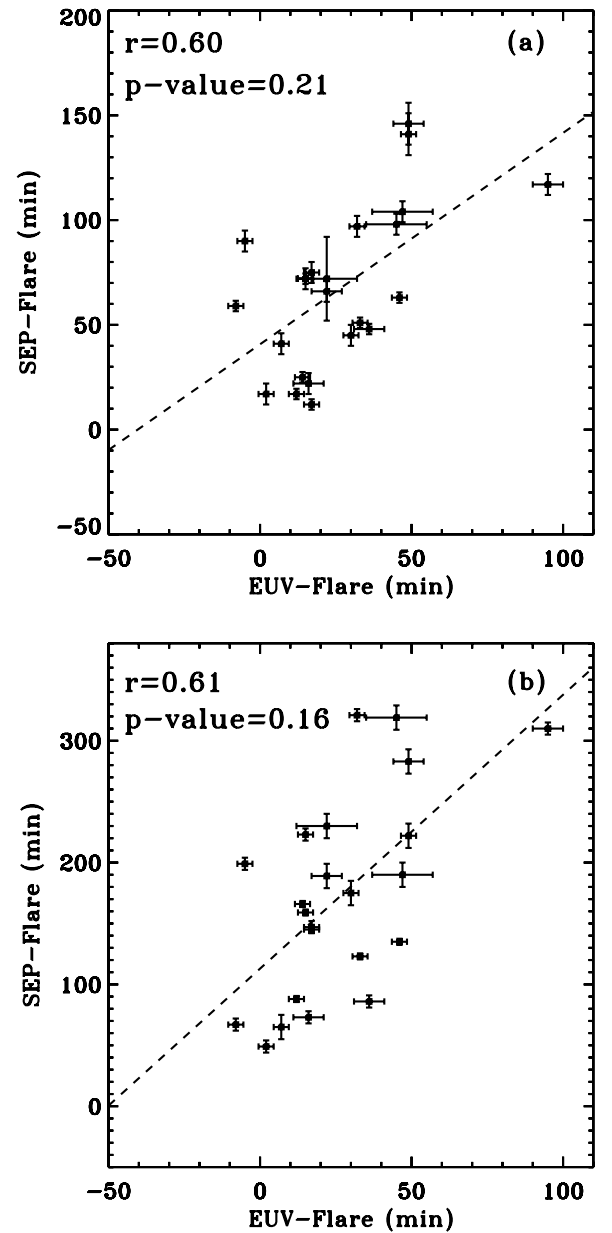


**Figure 11.** Relationship between EUV flare time and SEP flare time: (a) electron and (b) proton. The error bars represent the number of degradations. The dashed line is a linear least squares fit to the data. In the figure,  $r$  means a correlation coefficient and the  $p$ -value is the probability that  $r = 0$ .

at Earth, where the flux enhancement was slightly delayed (Figure 7). At this time, there were several ARs on the Sun. Three produced flares near the SEP onset time. AR 11339 (N18E60) was the site of an X-class flare (20:16 UT) near the connecting footpoint of *STB* about 3 hr before the SEP onset. There was no type III radio burst associated with the X-flare, suggesting that any particles produced by the X-flare were trapped close to the Sun. Later, around the time of the SEP onset, AR 11339 produced a C5.8 flare (22:28 UT) and this is the most likely source of the first SEPs detected by *STB*. Shortly afterward, a C9.2 flare (22:56 UT) and an M2.1 flare (23:28 UT) were seen from the same region and these probably further increased the SEP flux arriving at *STB*.

The most likely source of the SEP event seen at *STA* was a backside, from Earth, AR at N05E160 that was  $100^\circ$  east of the X-flare site with good connection to *STA* (Figure 8).

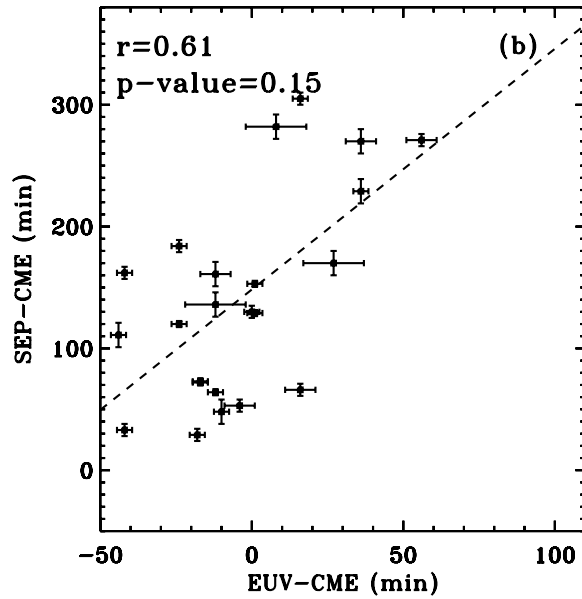
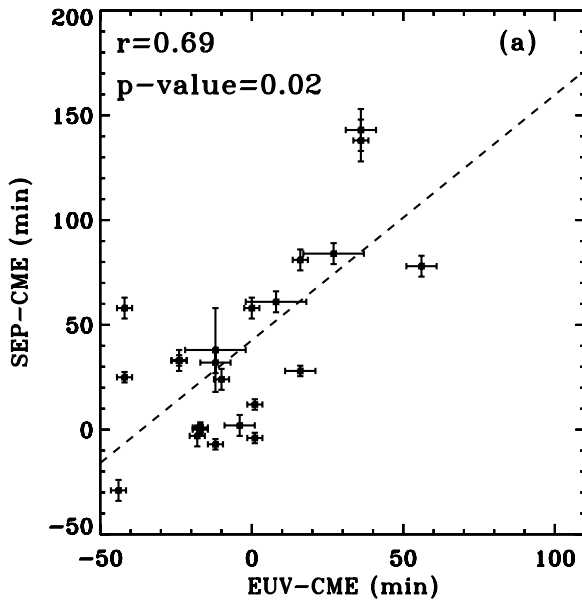


**Figure 12.** Relationship between EUV-CME time and SEP-CME time, as in Figure 10.

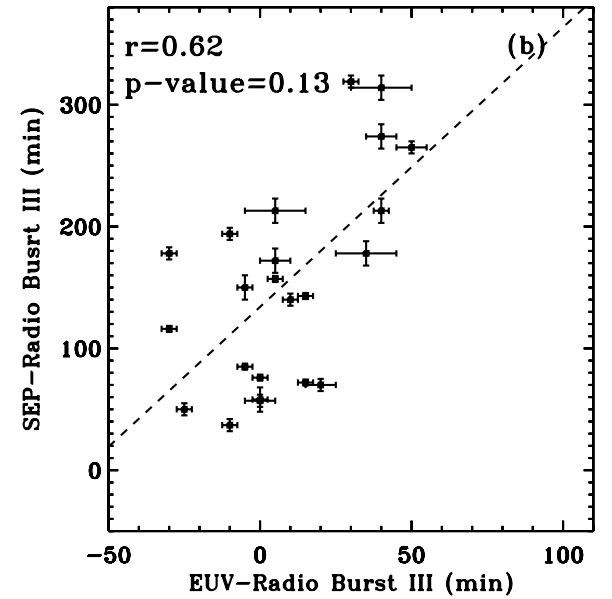
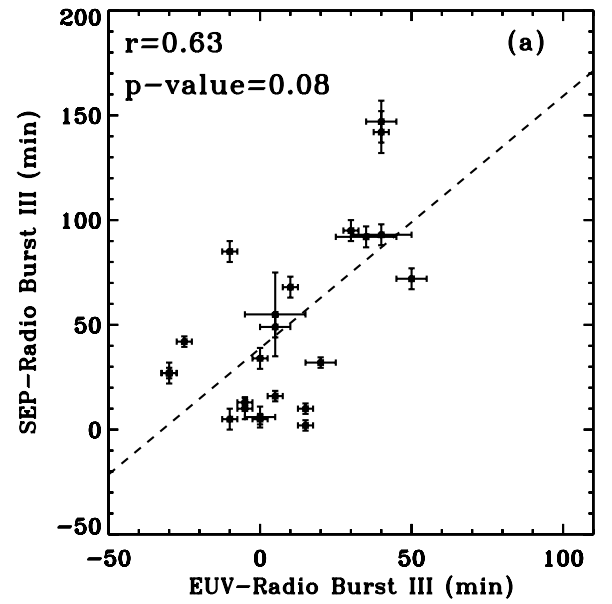


**Figure 13.** Relationship between EUV-radio burst III time and SEP-radio burst III time, as in Figure 10.

The brightening and EUV wave were first seen in *STEREO* images at 22:16 UT. The EUV wave propagated westward to the connecting footpoints of *STB* and eastward to the connecting footpoints of Earth. In the running ratio movie, it looks as though the EUV wave stopped at intervening ARs in both directions because it could not be traced beyond them. Several reports have shown that EUV waves are reflected and refracted by strong AR region magnetic fields (Thompson et al. 1999; Wang 2000; Ofman & Thompson 2002; Li et al. 2012b). If the CME shock continued to move horizontally at the velocity of the EUV wave ( $660 \text{ km s}^{-1}$ ), then it would have reached the *STB* footpoint (AR11339) at 22:25 UT. So, it could have triggered the C5.8 flare at 22:28 UT.

Close to the Earth footpoint, there was a C5.4 flare at 22:12 UT in AR11333 (N10W85) that may have produced some of the SEPs, particularly the early electrons, seen at Earth. Protons were detected at roughly the same time at Earth and *STA*, so the

most likely cause for these is the CME shock associated with the EUV wave from the flare near the *STA* footpoint at 22:16 UT.

### 3.2.3. The Event of 2011 November 26

Figure 9 shows the electron and proton fluxes at *STB*, Earth, and *STA* for the event of 2011 November 26. The fluxes enhanced first at Earth, then *STB*, and later in *STA*. The *STA* flux enhancements are larger than the *STB* enhancements and their increase is more gradual.

There are several ARs around the main SEP source region (AR 11353), as shown in Figure 10(a). Around the SEP onset time, a big filament eruption occurred, covering a large area across the northern and southern hemispheres around longitude W30. It ran from just northeast of AR 11353 (N08W49) to AR 11354 (S15W50) and produced a CME with velocity  $1007 \text{ km s}^{-1}$  at 07:12 UT and a type II radio burst at 07:15 UT. On the Sun, there was a C1.2 flare and faint EUV wave starting

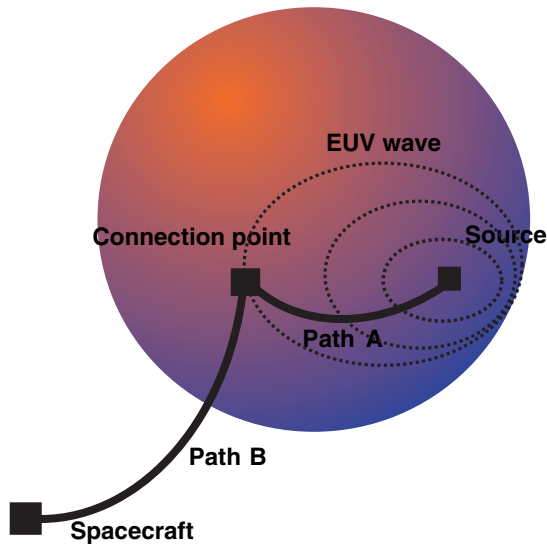


**Figure 14.** EUV wave trajectory from the source region to the connection point (path A) and SEP propagation from the connection point to the spacecraft (path B).

(A color version of this figure is available in the online journal.)

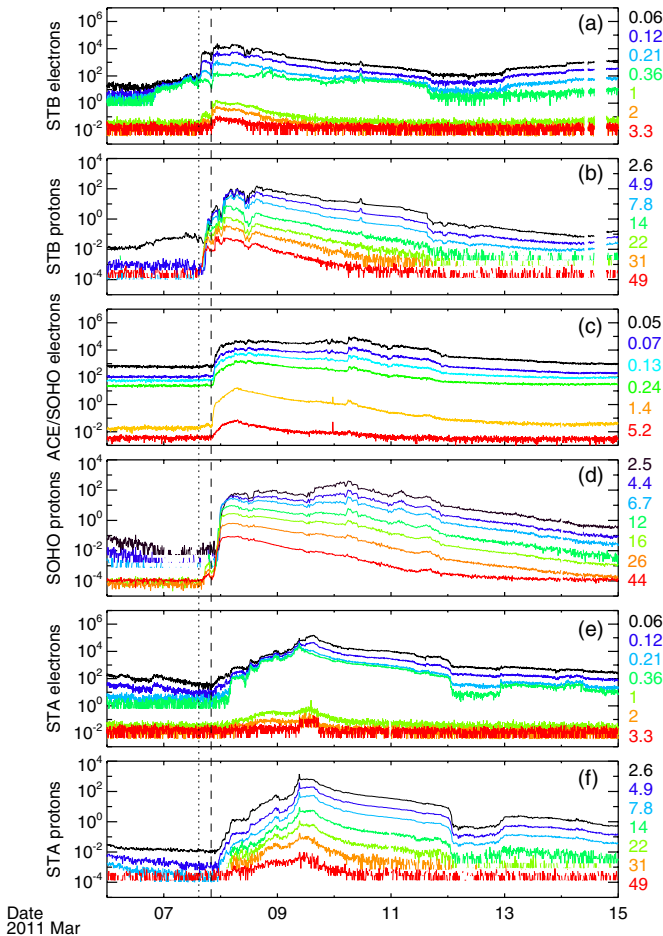


**Figure 15.** 2011 March 7 SEP event, as in Figure 1. The dashed line represents the CME at 20:00 UT on March 7. The dotted line is the CME at 14:48 UT on March 7. The rise in *STB* SEPT (low-energy) electron flux from about 12:00 UT on March 6 until the dotted line is due to ion contamination.

(A color version of this figure is available in the online journal.)

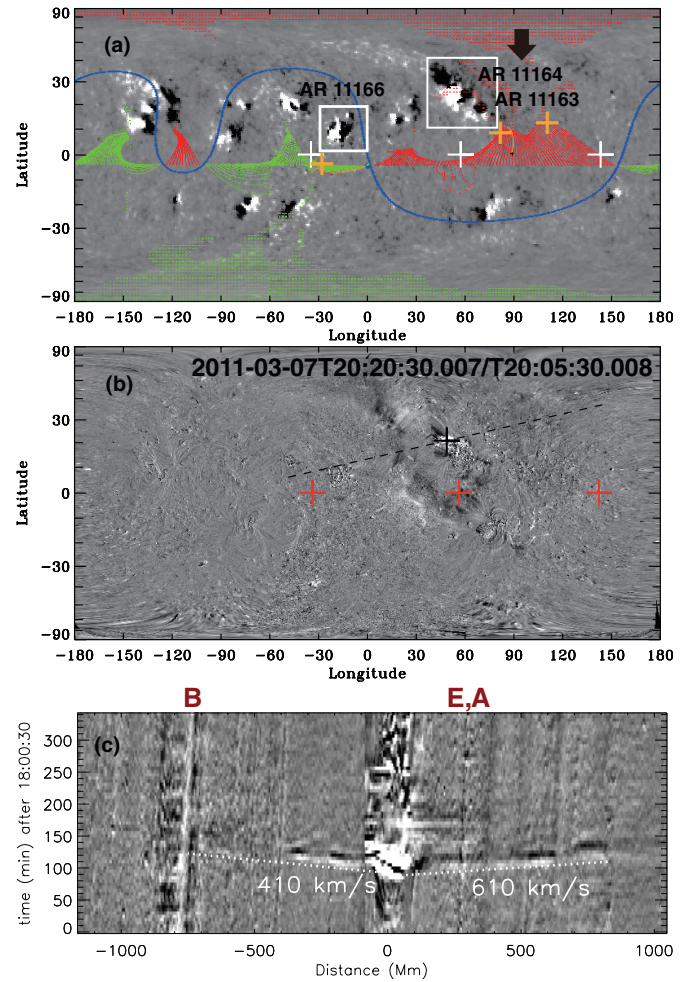


**Figure 16.** 2011 March 7 source sites and EUV wave. (a) GONG magnetic field map, as in Figure 2. The source of the first small CME was N11E14. The main CME was from N24W59. (b) Ratio of images at the given times, as in Figure 2. (c) Running ratio space-time image along the dashed line in (b).

(A color version of this figure is available in the online journal.)

at 06:40 UT (Figure 10(b)). To the northeast, the neighboring region AR 11360 (N17W00) produced a C4.9 flare and strong jet with velocity about  $150 \text{ km s}^{-1}$  from the edge of its sunspot at 08:10 UT (Figure 10(c)). The jet connected to the northern part of the filament eruption (AR 11355). At 08:16 UT, there was a brightening in the unmarked box in Figure 10(a).

In the synoptic ecliptic-plane field image shown in Figure 10(a), the ARs associated with the filament eruption surrounded the connection point of Earth. The electron arrival time at Earth (07:12 UT) is about 20 minutes later than expected for a direct connection. The electrons arrived at *STB* at 07:44 UT, which is consistent with them being accelerated at the edge of the EUV wave. The *STA* footprint is about 1000 Mm from the filament eruption site and the EUV wave could not be tracked that far. The weak and delayed detection of SEPs at *STA* is consistent with a very weak EUV wave front.

#### 4. SEP FLUX ENHANCEMENTS

We describe the SEP flux enhancements of 12 large SEP events in the context of the magnetic field connections from the solar sources to the spacecrafts, EUV wave propagation, and pre-event solar activity.

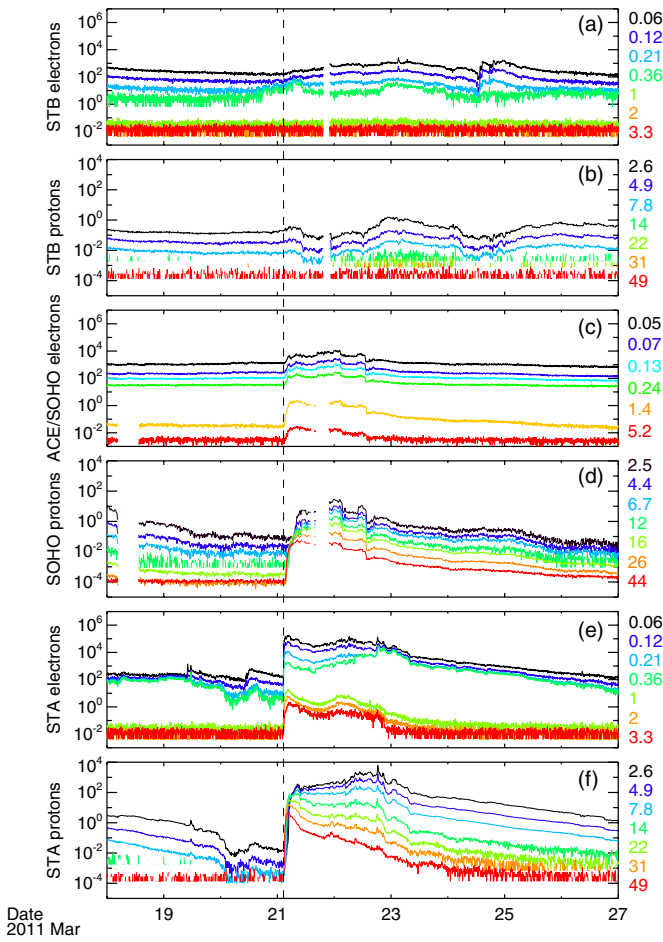


**Figure 17.** 2011 March 21 SEP event, as in Figure 1. The dashed line represents the CME at 02:24 UT on March 21. At *STB*, the flux variations are probably due to a passing interplanetary CME shocks on March 19 and 22 ([http://www-ssc.igpp.ucla.edu/forms/stereo/stereo\\_level\\_3.html](http://www-ssc.igpp.ucla.edu/forms/stereo/stereo_level_3.html)). The low-energy electron fluxes at *STB* were affected by ion contamination. This event has been studied by Rouillard et al. (2012).

(A color version of this figure is available in the online journal.)

#### 4.1. Direct Magnetic Field Connections

In all cases when the source regions were close to the connection footpoints of the spacecraft, the fluxes were strongly enhanced. In particular, the single source regions were directly connected to both *STB* and Earth on 2011 August 14 and to *STA* and Earth on August 18. The event of 2011 November 3 had three different sources and the sources were connected to *STA*, *STB*, and Earth. This is the only event where flux enhancements abruptly increased at all three positions.

The event of 2012 January 23 (Figures 22 and 23 in the Appendix) had no direct connections to the flare source (AR 11402), but the fluxes enhanced significantly in all three spacecraft. There were also other cases of flux enhancements without direct connections to the flare source (e.g., *STB* on 2010 August 18, *STA* and *STB* on 2011 March 7, Earth on 2011 March 21, *STA* on 2011 August 4, and *STA* on 2012 January 27).

In this study, seven events from single source regions and one event with multiple eruptions were well connected to one spacecraft, two events from single source regions were well connected to two spacecraft, and one event had no connection. Noticeably, the three source regions of one event are connected with three spacecraft, respectively.

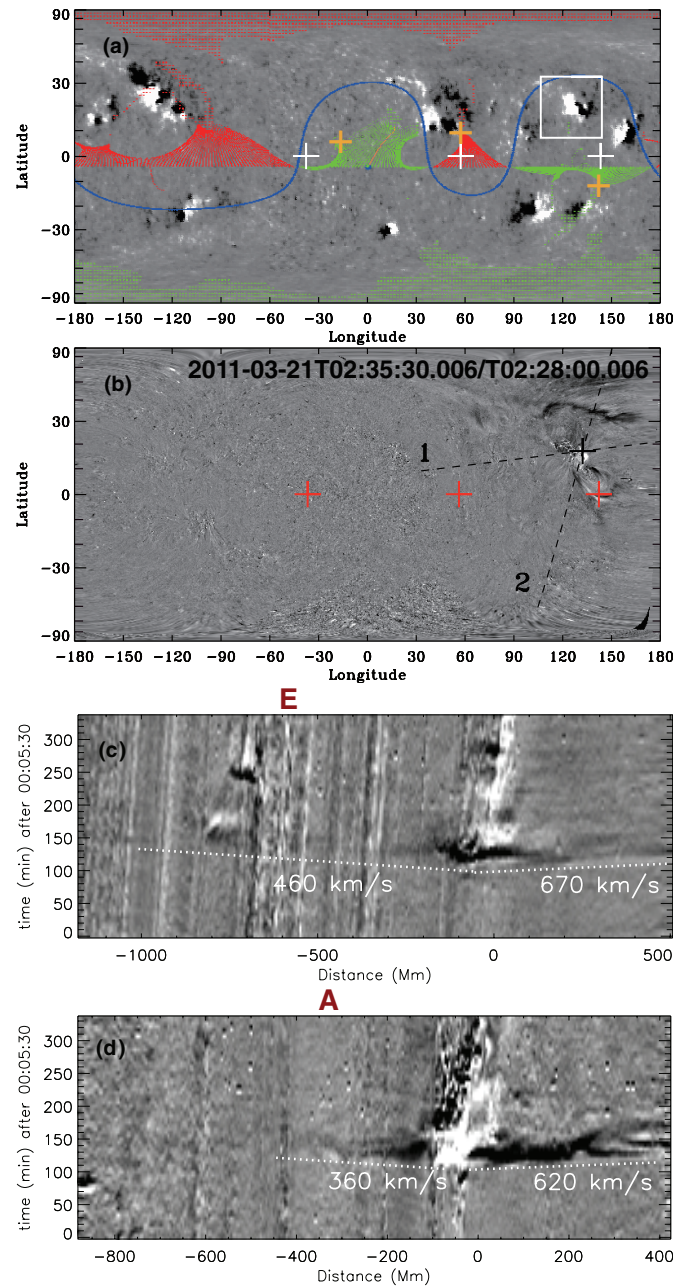


**Figure 18.** 2011 March 21 source site and EUV wave. (a) GONG magnetic field map, as described in Figure 2. (b) Ratio of images at the given times, as in Figure 2. (c) Running ratio space-time image along line 1 in (b). (d) Running ratio space-time image along line 2 in (b).

(A color version of this figure is available in the online journal.)

#### 4.2. EUV Wave Connection

EUV waves were seen in all the analyzed SEP events. The average velocity of the EUV waves is  $463 \text{ km s}^{-1}$ . The highest is  $760 \text{ km s}^{-1}$  and lowest is  $200 \text{ km s}^{-1}$  (Table 1). In general, the EUV waves could be tracked up to 1000 Mm or about a quarter of the distance around the Sun. Beyond that, they became faint, making it difficult to determine the time that the waves crossed the spacecraft connecting footpoint. Also, EUV waves may reflect at ARs (Li et al. 2012b), so when there were many ARs on the Sun it was difficult to track the EUV waves.

In this section, we compare the time at which an EUV wave reaches a spacecraft connection point with the time that the

**Table 4**  
The Linear Regression Coefficients for the Fits in Figures 10–12

	SEP	$a$	$\sigma_a$	$b$	$\sigma_b$	Figure
Flare	e	1.01	$\pm 0.30$	40.73	$\pm 10.17$	10(a)
	p	2.25	$\pm 0.64$	112.92	$\pm 22.01$	10(b)
CME	e	1.17	$\pm 0.27$	42.65	$\pm 6.95$	11(a)
	p	1.98	$\pm 0.56$	148.31	$\pm 14.31$	11(b)
Type III	e	1.20	$\pm 0.32$	38.79	$\pm 7.64$	12(a)
	p	2.30	$\pm 0.64$	134.06	$\pm 15.29$	12(b)

**Notes.** The equation is  $y = ax + b$ .  $\sigma_a$  and  $\sigma_b$  are the  $1\sigma$  uncertainty estimations of  $a$  and  $b$ . In Column 2, e means electron and p means proton.

spacecraft recorded the SEP onset. Our investigation covered 12 events and three spacecraft positions, so that in principle there were 36 cases. However, in practice, the EUVs could not always be tracked to the connecting footpoints of all spacecraft and in some events SEPs were not seen at all positions. There were seven cases where SEPs were recorded without EUV waves (i.e., *STB* on 2011 September 21, *STA* on September 22, *STB* and Earth on November 3, *STB* and *STA* on November 26, and *STA* on 2012 January 23).

To examine the relationship between EUV waves and SEP onset times, we need an offset time against which we can compare the SEP onset times at the spacecraft and EUV arrival times at the photospheric magnetic field connection points of the spacecraft. There are three natural choices: flare, CME, and type III radio burst times. Figures 11–13 show the relationships between the EUV wave travel times to the connecting footpoints (EUV arrival time – solar event time) and the SEP travel time (SEP onset time – solar event time). All cases have moderate correlation coefficients, stronger in the electron groups. The highest correlation value is 0.69 for electrons when the CME time is used (Figure 12(a)). Table 4 lists the slopes and offsets from the linear regressions of the six pairs of relationships given by Figures 11–13. The averages of the slopes and offsets are 1.1 and 40.7 minutes for electrons and 2.2 and 131.8 minutes for protons, respectively.

To interpret these numbers, we can consider two trajectories (Figure 14): the EUV wave trajectory (path A) on the solar surface and the SEP propagation trajectory in interplanetary space (path B). This assumes that the EUV wavefront tracks the skirt of the CME shock or the outer edge of the reconnection region behind the CME. In both cases, the EUV wave indicates the outer edge of SEPs associated with the CME. The SEPs travel along their local magnetic field lines. If the SEPs are generated on field lines connected to the spacecraft, they can be detected by that spacecraft. Consequently, the SEPs are detected with a delay time given by the time along path B and path A (time of path A + B). The slope of the correlations shows how the SEP onset delay changes with EUV wave travel time from its source region. The offset gives the travel times of electrons/protons from the connecting point to the spacecraft through interplanetary space.

Thus, if we assume this model, the electron travel times are essentially independent of the distance (slope 1.1) of the connecting footpoint from the flare site. The electron offset (40.7 minutes) is about 20 minutes longer than the travel times expected for 175 keV electrons along a path of 1.2 AU. Although this is consistent with previous observations (Haggerty & Roelof 2002; Klassen et al. 2002), the reasons are not understood (Vocks & Mann 2009). On the other hand, the proton delay time increases with distance (slope 2.2) and the proton offset is about

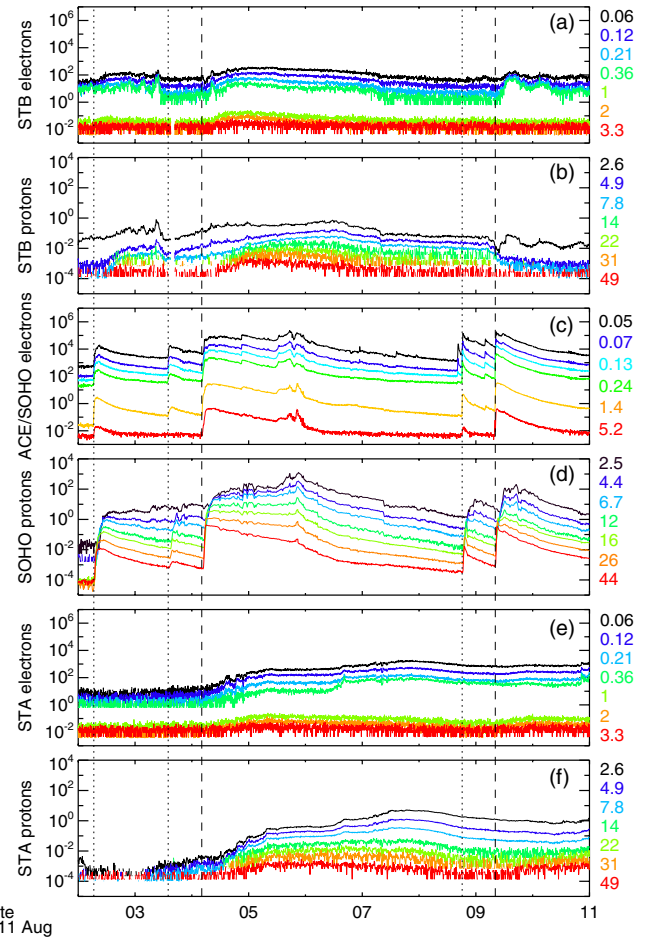


**Figure 19.** 2011 August 4 and 9 SEP events, as in Figure 1. The two dashed lines represent the CME at 03:54 UT on August 4 and the CME at 18:12 UT on August 8. The three dotted lines are the CMEs at 06:36 UT on August 2, 14:00 UT on August 3, and at 08:12 UT on August 9. On August 9, the low-energy SEP protons at *STB* were probably caused by a CIR and the enhancements in the electron channels were due to ion contamination.

(A color version of this figure is available in the online journal.)

30 minutes fewer than the expected travel time for 1.8 MeV protons, which is more than the uncertainty of the linear fits. The high value of the proton slope suggests that the protons are not well coupled to the EUV wave. Further, the low offset value suggests that the proton travel time increase is faster than linear with the travel time of the EUV wave to the connecting footpoint because then the offset of the linear fit would be lower than expected.

#### 4.3. Pre-event Solar Activity

In this study, four SEP events were possibly related to pre-event activity that occurred less than 1 day before the event. The event on 2011 March 7 (Figures 15 and 16 in the Appendix) was related to two CMEs. The first, with  $698 \text{ km s}^{-1}$  at 14:48 UT, was associated with an M1.7 flare in N11E14 and produced flux enhancements only at *STB*. The second CME at 20:00 UT had its source site  $70^\circ$  to the west at N24W59. It had the highest velocity in our study ( $2256 \text{ km s}^{-1}$ ) and flux enhancements were recorded at all spacecraft. It is likely that the first CME influenced the SEP propagation from the second.

The event of 2011 August 4 (Figures 19 and 20 in the Appendix) was related to a CME from N15W49 with  $1785 \text{ km s}^{-1}$  at 03:54 UT. Before the event, CMEs occurred

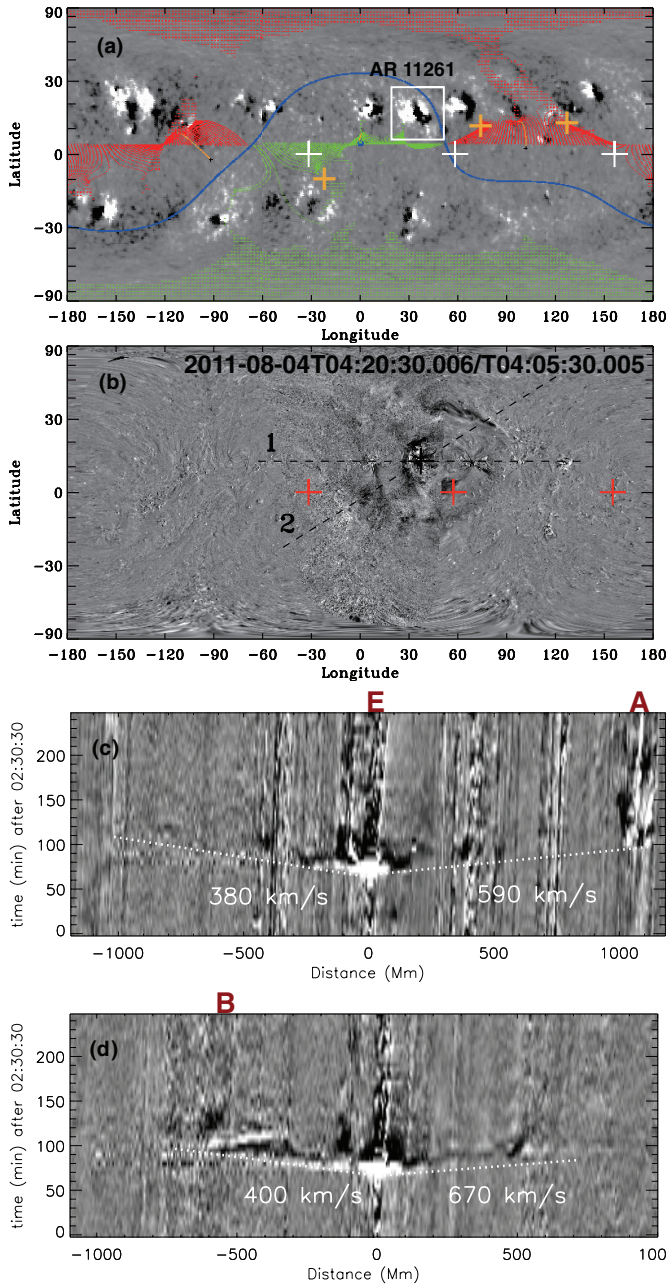


**Figure 20.** 2011 August 4 source site and EUV wave. (a) GONG magnetic field map as described in Figure 2. The CMEs on August 2–4 are from the source region enclosed by the white square. (b) Ratio of images at the given times, as in Figure 2. (c) Running ratio space–time image along line 1 in (b). (d) Running ratio space–time image along line 2 in (b).

(A color version of this figure is available in the online journal.)

from the same AR with  $610 \text{ km s}^{-1}$  at 14:00 UT on August 3 (M6.0) and with  $712 \text{ km s}^{-1}$  at 06:36 UT on August 2 (M1.4).

The events on 2011 August 8 and 9 (Figures 19 and 21 in the Appendix) were interesting because there were two fast ( $1343 \text{ km s}^{-1}$  and  $1610 \text{ km s}^{-1}$ ) CMEs related to an M3.5 and an X6.9 flare from the same AR (AR 11263, N18W84), but SEP enhancements were only strong at Earth in spite of there being low background, at least at high energies, at *STB* and *STA*. The CME on the August 9 also produced a type II radio burst so it may have been expected to have produced a wide shock and spread of SEPs. Maybe the reason that SEPs were barely detected at *STB* and *STA* was related to the weak EUV wave in

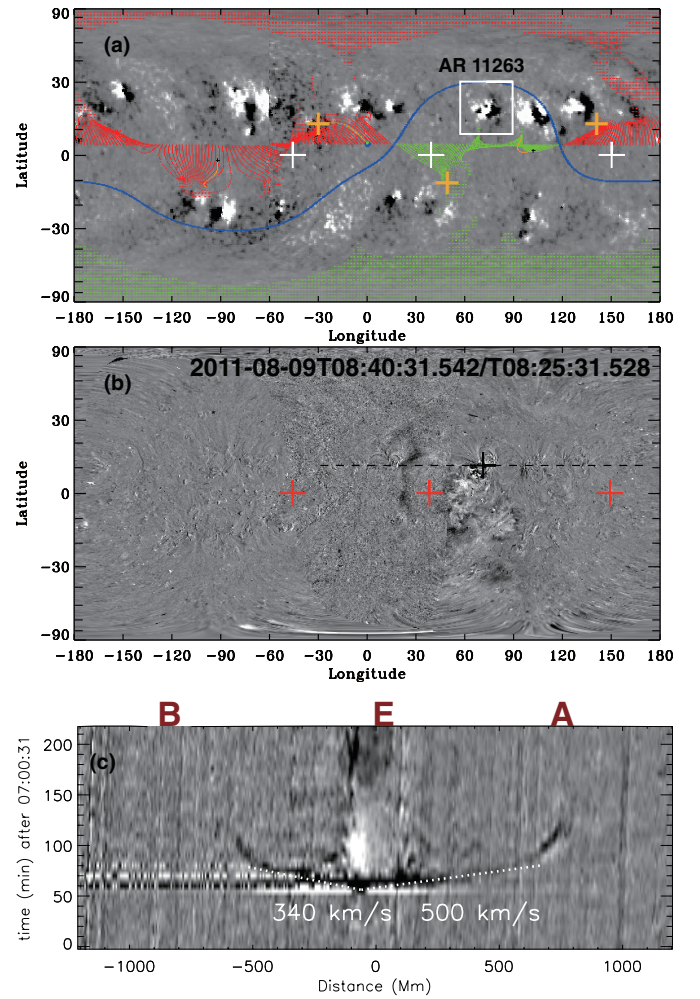


**Figure 21.** 2011 August 9 source site and EUV wave. (a) GONG magnetic field map, as described in Figure 2. The CMEs on August 8 and 9 are from the source region enclosed by the white square. (b) Ratio of images at the given times, as in Figure 2. (c) Running ratio space–time image along line 1 in (b).

(A color version of this figure is available in the online journal.)

the direction of the *STB* and *STA* connecting points (Figure 21(c) in the Appendix). There were weak *STA* electron enhancements at higher energies.

The event of 2011 September 22 (Section 3.2.1) may have been influenced by the CME with  $1007 \text{ km s}^{-1}$  that occurred at 22:12 UT on September 21 and caused electron and proton flux enhancements on *STA*, although the two events were on either side of the Sun. The event on September 22 was associated with a fast CME ( $1905 \text{ km s}^{-1}$ ) and strong flux enhancements in *STB* and slightly later at Earth and *STA*. There was a third brightening at 11:15 UT seen from *STA* that may have contributed to the flux enhancement at *STA*.

## 5. SUMMARY

We have studied the source regions of 12 SEP events from 2010 August to 2012 January using widely separated multiple spacecraft. For the analysis of the source site and related EUV waves, we used EUVI/AIA Stonyhurst Heliographic images. Also, we deduced the spacecraft photospheric connection points on the Sun using synoptic ecliptic-plane PFSS images. We have interpreted SEP flux enhancements with the magnetic

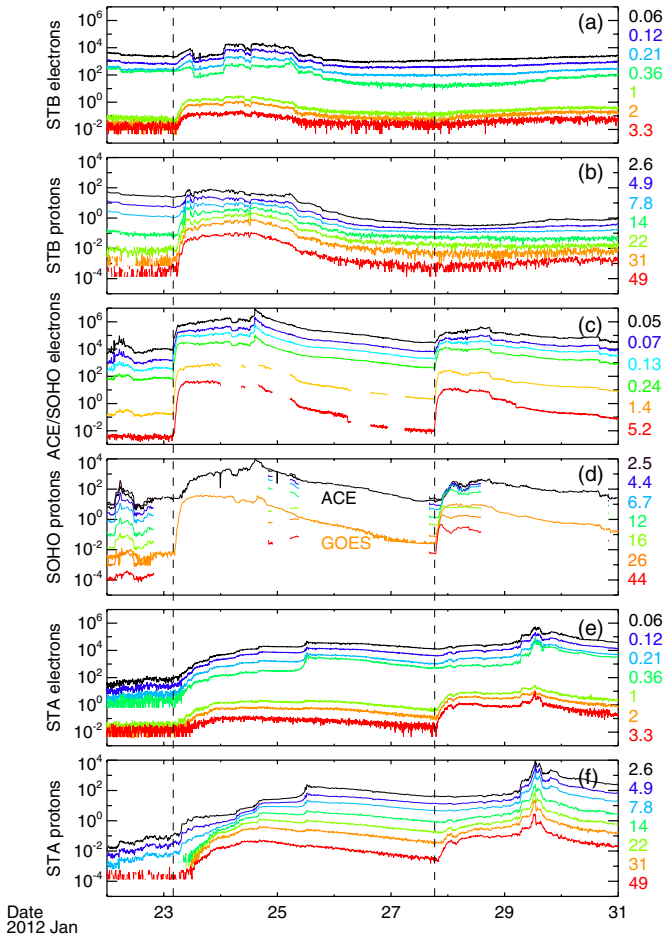


**Figure 22.** 2012 January 23 and 27 SEP events, as in Figure 1. In addition, in (d) we show the *ACE* 1.89–4.75 MeV and *GOES* > 30 MeV proton fluxes. The first dashed line represents the CME at 03:54 UT on January 23 and the second dashed line is the CME at 18:27 UT on January 27.

(A color version of this figure is available in the online journal.)

field connections, EUV waves, and pre-event activity at widely separated positions.

From this study, we have found that nine events were related to a single source region and the other three were probably due to multiple sources. Five events had strong flux enhancements in all three spacecraft.

Eruptions from multiple source regions sometimes cause abrupt flux enhancements simultaneously at widely separated positions. The most notable event was likely the one on 2011 November 3 that showed abrupt enhancements at *STB*, Earth, and *STA*. There may have been three different sources that erupted at almost the same time and were connected to *STB*, Earth, and *STA* but one needs to look at coronagraph data to identify the SEP sources. This will be done in a follow-up analysis. Another unusual event possibly related to multiple sources was the event on 2011 November 26. First, a large transequatorial filament erupted with good connection to Earth. Later, neighboring ARs produced a jet and small flare connected to *STB* and *STA*, respectively. In particular, the source region was the biggest in our study and the solar activities associated with the event had a long duration ( $\sim 100$  minutes).

In all the SEP events, EUV waves (average speed  $\sim 463$  km s $^{-1}$ ) were observed with fast CMEs (average speed  $\sim 1470$  km s $^{-1}$ ). To examine the relationship between EUV waves and the sites of SEP acceleration, we have considered

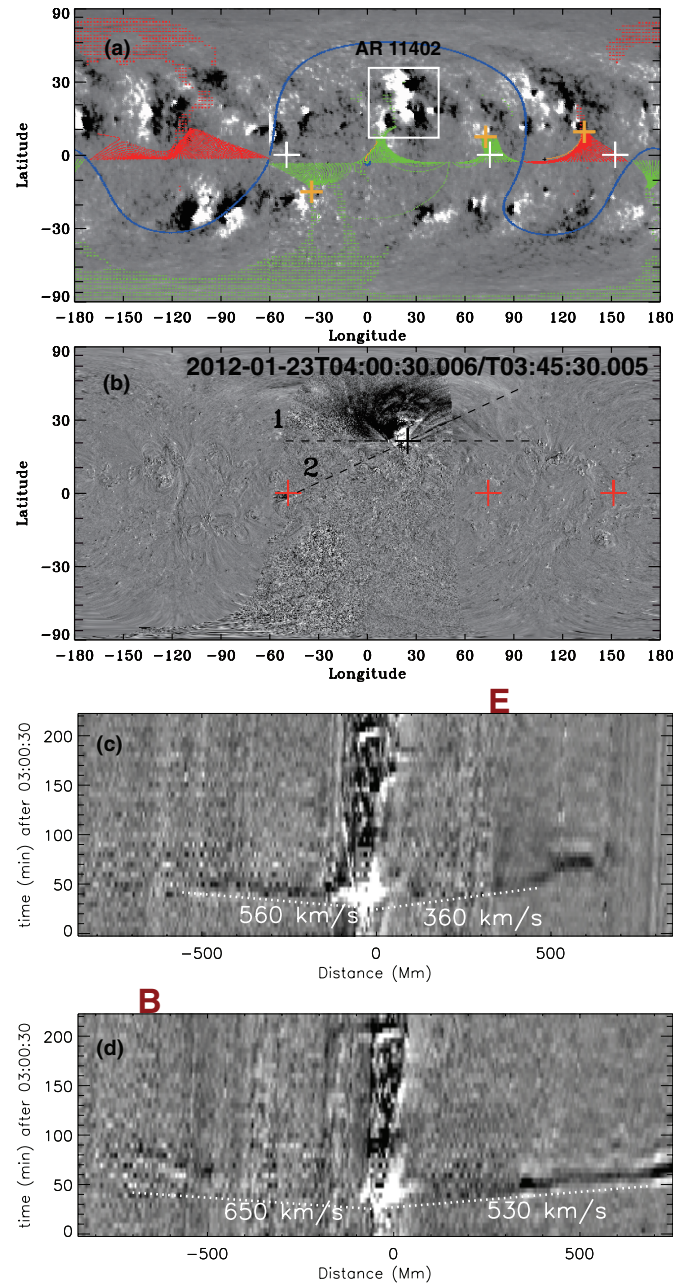


**Figure 23.** 2012 January 23 source site and EUV wave. (a) GONG magnetic field map, as described in Figure 2. (b) Ratio of images at the given times, as in Figure 2. (c) Running ratio space-time image along line 1 in (b). (d) Running ratio space-time image along line 2 in (b).

(A color version of this figure is available in the online journal.)

an offset time using flare, CME, and type III radio burst times against which we can compare the SEP onset and EUV arrival times. SEP onset times are significantly associated with EUV wave arrival times. Our result shows that the correlation coefficients between the two parameters are between 0.60 and 0.69 (Figures 10–12). The results support the idea that EUV waves trace the release sites of SEPs, which is consistent with previous studies that suggested that SEPs are accelerated by large coronal shock waves (Kocharov et al. 1994; Torsti et al. 1998; Krucker et al. 1999; Vainio & Khan 2004; Rouillard et al. 2012).

In this study, most events were associated with complex solar sources and flux enhancements. Although direct open magnetic field connections play an important role in generating SEP

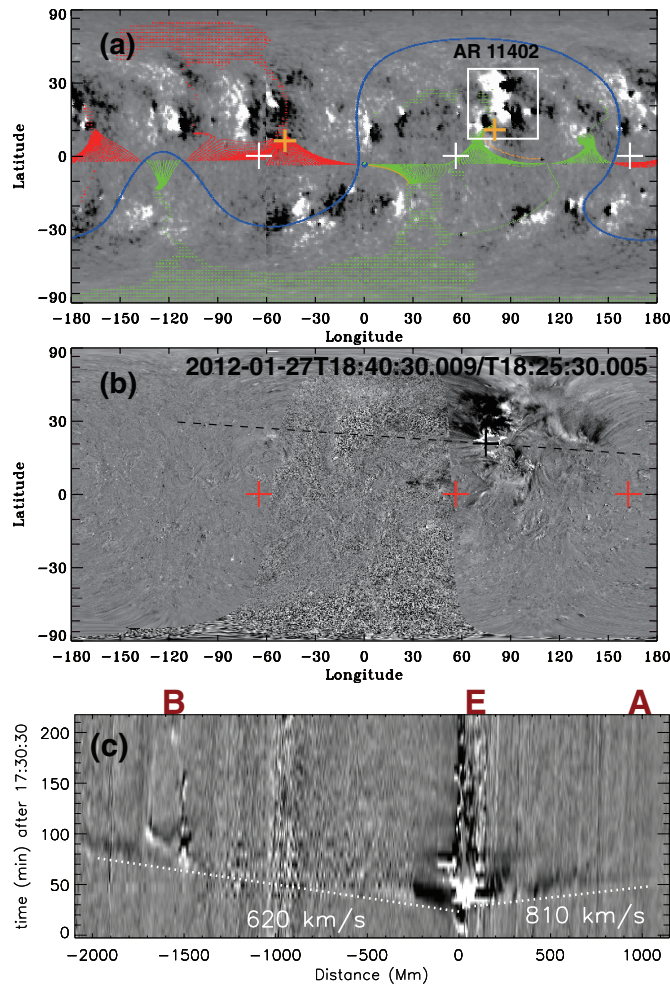


**Figure 24.** 2012 January 27 source site and EUV wave. (a) GONG magnetic field map, as described in Figure 2. (b) Ratio of images at the given times, as in Figure 2. (c) Running ratio space-time image along line 1 in (b).

(A color version of this figure is available in the online journal.)

events with strong flux enhancements, in our study, the flux enhancements were observed in 19 electron cases and 14 proton cases without magnetic field connections. Kozarev et al. (2011) found that protons that came from a site with an open field geometry were quickly accelerated into interplanetary space, while protons associated with a closed field geometry were probably accelerated in shocks. The fact that all strong events reported in our study were associated with type II radio emission supports the idea that the SEP events were generated by CME-driven shocks. The observations of the flux enhancements show that the shocks can spread over at least  $\sim 180^\circ$ .

We thank the referee for constructive comments and we thank the *SDO/AIA* and *STEREO/EUVI* teams for the remarkable data. This work has been supported by AOARD (FA2386-13-1-4066), by the BK21 plus program through the National Research Foundation (NRF) funded by the Ministry of Education of Korea, and by the Korea Research Foundation Grant funded by the Korean Government (20100014501 and 2013042232). This

work was also supported by the Construction of Korean Space Weather Center and the project of KASI. The work at MPI was supported by the Bundesministerium für Wirtschaft under grant 50 OC 0904.

## APPENDIX

This Appendix shows SEP fluxes, the synoptic ecliptic-plane PFSS images, the running ratio image, and the running ratio space-time plots on the event of 2011 March 7 (Figures 15 and 16), the event of 2011 March 21 (Figures 17 and 18), the event of 2011 August 4 (Figures 19 and 20), the event of 2011 August 9 (Figures 19 and 21), the event of 2012 January 23 (Figures 22 and 23) and 27 (Figures 22 and 24). The figures are available in the online version.

## REFERENCES

- Attrill, G. D. R., Harra, L. K., van Driel-Gesztelyi, L., & Démoulin, P. 2007, *ApJL*, **656**, L101
- Cane, H. V., McGuire, R. E., & von Rosenvinge, T. T. 1986, *ApJ*, **301**, 448
- Cheng, X., Zhang, J., Olmedo, O., et al. 2012, *ApJL*, **745**, L5
- Dresing, N., Gómez-Herrero, R., Klassen, A., et al. 2012, *SoPh*, **281**, 281
- Galvin, A. B., Kistler, L. M., Popecki, M. A., et al. 2008, *SSRv*, **136**, 437
- Gold, R. E., Krimigis, S. M., Hawkins, S. E., III., et al. 1998, *SSRv*, **86**, 541
- Gopalswamy, N., Yashiro, S., Krucker, S., Stenborg, G., & Howard, R. A. 2004, *JGRA*, **109**, 12105
- Haggerty, D. K., & Roelof, E. C. 2002, *ApJ*, **579**, 841
- Kahler, S. W. 2005, *ApJ*, **628**, 1014
- Kallenrode, M.-B. 2003, *JPhG*, **29**, 965
- Klassen, A., Bothmer, V., Mann, G., et al. 2002, *A&A*, **385**, 1078
- Kocharov, L. G., Lee, J. W., Zirin, H., et al. 1994, *SoPh*, **155**, 149
- Kozarev, K. A., Korreck, K. E., Lobzin, V. V., Weber, M. A., & Schwadron, N. A. 2011, *ApJL*, **733**, L25
- Krucker, S., Larson, D. E., Lin, R. P., & Thompson, B. J. 1999, *ApJ*, **519**, 864
- Lario, D., Aran, A., Gómez-Herrero, R., et al. 2013, *ApJ*, **767**, 41
- Li, G., Moore, R., Mewaldt, R. A., Zhao, L., & Labrador, A. W. 2012a, *SSRv*, **171**, 141
- Li, T., Zhang, J., Yang, S., & Liu, W. 2012b, *ApJ*, **746**, 13
- McComas, D. J., Bame, S. J., Barker, P., et al. 1998, *SSRv*, **86**, 563
- Mewaldt, R. A., Cohen, C. M. S., Cook, W. R., et al. 2008, *SSRv*, **136**, 285
- Müller-Mellin, R., Böttcher, S., Falenski, J., et al. 2008, *SSRv*, **136**, 363
- Müller-Mellin, R., Kunow, H., Fleißner, V., et al. 1995, *SoPh*, **162**, 483
- Neugebauer, M., Forsyth, R. J., Galvin, A. B., et al. 1998, *JGR*, **103**, 14587
- Nitta, N. V., Liu, Y., DeRosa, M. L., & Nightingale, R. W. 2012, *SSRv*, **171**, 61
- Ofman, L., & Thompson, B. J. 2002, *ApJ*, **574**, 440
- Patsourakos, S., & Vourlidas, A. 2009, *ApJL*, **700**, L182
- Reames, D. V. 1999, *SSRv*, **90**, 413
- Reames, D. V., Ng, C. K., & Tylka, A. J. 2012, *SoPh*, **285**, 283
- Rouillard, A. P., Sheeley, N. R., Tylka, A., et al. 2012, *ApJ*, **752**, 44
- Thompson, B. J., Gurman, J. B., Neupert, W. M., et al. 1999, *ApJL*, **517**, L151
- Thompson, B. J., & Myers, D. C. 2009, *ApJS*, **183**, 225
- Torsti, J., Anttila, A., Kocharov, L., et al. 1998, *GeoRL*, **25**, 2525
- Torsti, J., Kocharov, L. G., Teittinen, M., & Thompson, B. J. 1999, *ApJ*, **510**, 460
- Torsti, J., Valtonen, E., Lumme, M., et al. 1995, *SoPh*, **162**, 505
- Tylka, A. J., Malandraki, O. E., Dorrian, G., et al. 2012, *SoPh*, **285**, 251
- Vainio, R., & Khan, J. I. 2004, *ApJ*, **600**, 451
- Veronig, A. M., Muhr, N., Kienreich, I. W., Temmer, M., & Vršnak, B. 2010, *ApJL*, **716**, L57
- Vocks, C., & Mann, G. 2009, *A&A*, **502**, 325
- von Rosenvinge, T. T., Reames, D. V., Baker, R., et al. 2008, *SSRv*, **136**, 391
- Wang, Y.-M. 2000, *ApJL*, **543**, L89
- Warmuth, A. 2010, *AdSpR*, **45**, 527
- Warmuth, A., & Mann, G. 2011, *A&A*, **532**, A151
- Wuelser, J.-P., Lemen, J. R., Tarbell, T. D., et al. 2004, *Proc. SPIE*, **5171**, 111